ICRF Heating In the WVII-A Stellarator

G. CATTANEI, ICRH TEAM, W VII-A TEAM, NI TEAM

IPP 2/290 October 1987

MAX-PLANCK-INSTITUT FÜR PLASMAPHYSIK

8046 GARCHING BEI MÜNCHEN

MAX-PLANCK-INSTITUT FÜR PLASMAPHYSIK

GARCHING BEI MÜNCHEN

ICRF Heating In the WVII-A Stellarator

G. CATTANEI, ICRH TEAM, W VII-A TEAM, NI TEAM

IPP 2/290 October 1987

Die nachstehende Arbeit wurde im Rahmen des Vertrages zwischen dem Max-Planck-Institut für Plasmaphysik und der Europäischen Atomgemeinschaft über die Zusammenarbeit auf dem Gebiete der Plasmaphysik durchgeführt.

IPP 2/290 G. CATTANEI,
ICRH TEAM,
W VII-A TEAM,
NI TEAM

ICRF Heating In the W VII-A Stellarator

Abstract

The problem of ICRF wave propagation in an inhomogeneous toroidal plasma is analysed in some detail, and rf power deposition profiles in the W VII-A stellarator plasma are numerically evaluated.
The two antennas used in the W VII-A stellarator are then described and a self-consistent evaluation of their plasma loaded impedance is given.
Finally, the experimental results are analysed and an attempt is made to compare them, at least qualitatively, with the theoretical predictions, even though effective plasma heating was always overshadowed by a massive increase in radiation losses.

1. Introduction

ICRF heating could be a very welcome method to heat the plasma of the W VII-A and W VII-AS stellarators. Compared with NI, it has the advantage that the plasma density does not necessarily increase during the heating process. This could be essential in the standard case of an ECRF heated plasma since then the plasma density could be kept below the cut-off of the ECRF wave ($n_e \approx 6\ 10^{13}\ cm^{-3}$ for the gyratron frequency f = 70 GHz) and ions and electrons could be heated independently.
The main effect which limits the efficency of ICRF heating is impurity production. Owing to the bad surface-to-volume ratio, this limit is much more severe in small-size plasmas, as shown by earlier ICRF heating experiments in small tokamaks, such as ST /1/ ,TM1-RF /2/ and T01 /3/, where the rf energy coupled to the plasma was severely limited (E $\leq$ 100 J) by a large increase of the impurity content. The main source of impurities is commonly attributed to badly confined energetic ions striking the wall. Since energetic ions in the W VII-A stellarator are well confined only in a small region close to to the axis, owing to its small dimensions, a large increase in the impurity content and large radiative losses can be expected. Nevertheless, in view of its more promising application in the W VII-AS stellarator, an ICRF heating experiment was started in the W VII-A stellarator.
In the first part of this paper we consider at some length the problem of wave propagation in an inhomogeneous toroidal plasma when the plasma dimensions are too small to allow such approximations as required by ray-tracing or by other approximate methods such as matching asymptotic solutions. We start here with the full set of Maxwell's equations and consider an axisymmetric system . Note that to neglect toroidal gradients could be a rather poor approximation of the actual stellarator plasma in the case of very small wave damping, e.g. for second-harmonic heating, since then cavity modes would play an important role. We consider here, however, minority heating and/or mode conversion, in which case the wave damping is expected to be large enough for cavity modes to be unimportant. We take into account magnetic field gradients along the line of force but neglect electron inertia and finite ion Larmor radius; instead, when considering pure mode conversion, i.e. when the ion cyclotron layer is outside the plasma volume, we introduce a small collisional damping in order to avoid the singularity at the mode conversion layer.
In the second part we describe the two antennas which have been designed for the W VII-A stellarator and outline the method used to evaluate self-consistently the k_ϕ spectrum coupled by the two antennas and their plasma loaded impedance.
In the final part the experimental results are analysed in some detail, although the more or less effective plasma heating was always overshadowed by a strong increase in the impurity content, so that the total plasma energy content was, at least for longer rf pulses $\tau > 10\ ms$, lower at the end of the rf pulse than at the start.

2. Wave Propagation in a Non-uniform Plasma. Full Wave Theory.

We approximate the toroidal plasma by a straight plasma cylinder. It is required, however, that all quantities be periodic in z with period $2\pi R$, R being the major radius of the torus.
We assume further :

$$
\begin{aligned}
&a) \quad \vec{B} = \vec{e}_z B_o(1 - r/R\cos\theta) + \vec{e}_\theta B_o r/qR \\
&b) \quad m_e/m_i \to 0; \qquad \rho_i \to 0 \qquad r/R \ll 1; \\
&c) \quad n_e = n_e(r) \quad for \quad r \le s \quad and \quad n_e = 0 \quad for \quad r > s \\
&d) \quad \vec{E}(r,\theta,z) = \sum_m \vec{E}_m(r) \cdot exp\{i(m\theta + N\phi - \omega t)\} \qquad \phi = z/R
\end{aligned} \tag{1}
$$

We introduce rotating coordinates for the perpendicular components of the electric field: $E_m^{\pm} = E_r \pm iE_\xi$, where $E_\xi \approx E_\theta - (r/qR)E_z$, so that, neglecting terms of order r/R with respect to unity, we can write the plasma currents J_p in the form

$$
\begin{aligned}
J_m^- &= \sigma^-(r) \cdot E_m^- \\
J_m^+ &= \sum_n \sigma_{m,n}^+(r) \cdot E_n^+ \\
J_{//} &= \sigma_{//}(r) \cdot E_{//}
\end{aligned} \tag{2}
$$

where $\vec{J} = 4\pi i\omega \vec{J}_p/c^2$. If electron inertia is neglected, it follows that $\sigma_{//} \to \infty$, so that $E_{//} \approx 0$, $E_z \approx -(r/qR)E_\theta$ and $E_\xi \approx E_\theta$.
From Maxwell's equations one then has

$$
\frac{B_m}{r}\frac{d}{dr}\left(\frac{r}{B_m}\frac{d}{dr}\Psi_m\right) - \left(\frac{(m+1)^2}{r^2} + K_m(r)\right)\Psi_m = -B_m E_m^+ \tag{3}
$$

where

$$
\begin{aligned}
B_m &= C_m^2 + (m/r)dC/dr \\
K_m &\approx 2C_m \\
C_m &= k_{//}^2 - \sigma_-(r) \qquad k_{//} = N/R + m/qR \\
\Psi_m &= \sum_n T_{m,n} E_n^+ \\
T_{m,n} &= \{k_{//}^2 - \frac{1}{2}\sigma_-(r)\}\delta_{(m,n)} - \frac{1}{2}\sigma_{m,n}^+(r)
\end{aligned} \tag{4}
$$

We assume a two-ion component plasma $n_e = n_d + n_h$. Neglecting terms of order r/R with respect to unity, we have

$$
\sigma^-(r) \approx \frac{\Pi_d^2}{c^2}\frac{\omega^2}{\Omega_d(\omega + \Omega_d)} + \frac{\Pi_h^2}{c^2}\frac{\omega^2}{\Omega_h(\omega + \Omega_h)} \tag{5}
$$

where $\Omega_j = q_j B_o/m_j c$ is the ion cyclotron frequency at r=0 and $\Pi_j = \sqrt{4\pi q_j^2 n_j/m_j}$ is the ion plasma frequency.
We now consider two heating mechanisms :

a) Minority Heating: In this case we assume $\omega = \Omega_h$ and $n_h/n_d \ll s/R$. From /4/ we have

$$\sigma^+_{m,n} \approx \frac{\Pi_d^2}{c^2}\frac{\omega^2}{\Omega_d(\omega-\Omega_d)}\delta_{m,n} + i\frac{R}{r}\frac{\Pi_h^2}{c^2}\sqrt{\pi\mu}\, I_{\frac{(m-n)}{2}}(\frac{\mu}{2})\, exp\{i|m-n|\frac{\pi}{2} - \frac{\mu}{2}\} \tag{6}$$

where $\mu = (r/\rho_h)^2/\{N + (m+n)/2q\}^2$. Or, for $\mu \gg |m-n|$,

$$\sigma^+_{m,n} \approx \frac{\Pi_d^2}{c^2}\frac{\omega^2}{\Omega_d(\omega-\Omega_d)}\delta_{m,n} + i\frac{R}{r}\frac{\Pi_h^2}{c^2} exp\{i|m-n|\frac{\pi}{2} - (\frac{m-n}{2})^2(N+\frac{m+n}{2q})^2(\frac{\rho_h}{r})^2\} \tag{7}$$

b) Mode conversion: in this case we assume $\Delta = R(\Omega_h - \omega)/\omega > s$ and $n_h/n_d \geq s/R$, s being the antenna radius. We then have

$$\sigma^+_{m,n} \approx \frac{\Pi_d^2}{c^2}\frac{\omega^2}{\Omega_d(\omega-\Omega_d)}\delta_{m,n} + \frac{R}{\sqrt{\Delta^2+r^2}}\frac{\Pi_h^2}{c^2}\left(\frac{\Delta}{r} - \sqrt{(\frac{\Delta}{r})^2 - 1}\right)^{|m-n|} \tag{8}$$

Since $\sigma^+_{m,n}$ is now real, a surface $r = r^*$ can exist for which $T(r^*) = 0$, T(r) being the determinant of $T_{m,n}$.
From $E_m = \{\sum_n T^{-1}_{(m,n)}\Psi_n\}/T(r)$ it then follows that eq. (2) has a singularity at $r = r^*$. This singularity would of course disappear if terms proportional to ρ_d^2 or to m_e/m_i had been retained in the equations and the wave would, in general, be mode-converted to a kinetic wave. Since, however, these terms have been neglected here, a small collisional damping ($\omega = \omega + i\nu$, $\nu \ll \omega$) has been assumed in order to avoid the singularity at $r = r^*$. Physically, this corresponds to assuming that the rf power is entirely absorbed in the vicinity of the mode conversion layer, and to neglecting the possibility that a kinetic wave propagates away from the mode conversion layer. Note, however, that the total rf power absorbed by the plasma is given correctly in spite of our approximation, and that it will be independent of the magnitude of the collisional term, provided that ν is sufficently small.
We now assume the wave to be excited by an external current of the form

$$\vec{J}^{ext}(r,\theta,\phi) = = J_o\, \{\vec{e}_\theta\, U(\theta,\theta_1,\theta_2)\, \delta(r-s) - \vec{e}_r\, (\, \delta(\theta-\theta_2) - \delta(\theta-\theta_1))\, U(r,s,w)\}\, exp\{-i\omega t\} \tag{9}$$

where $U(x,a,b) = 1$ if $a \leq x \leq b$ and zero otherwise, and investigate two antennas:
Ant. I is fed at $\theta_1 = \pi/4$ and short circuited at $\theta_2 = -\pi/4$. This antenna couples the wave entirely from the low-magnetic-field side.
Ant. II is fed at $\theta_1 = \pi/4$ and short-circuited at $\theta_2 = \pi$, and thus in part couples the wave from the high-field side.
The set of eqs. (2) to (3) (truncated) have been integrated numerically with the proper boundary conditions at r = 0, r = s and $r = w$, where a perfectly conducting wall is assumed. The density profile of Fig. (6) and the following parameters have been assumed: R = 200 cm (major radius), s = 14 cm (coil radius), B = 2.5 T (magnetic field strength) and $T_h = T_d = T_e = 400\ eV$ (ions and electron temperature).

a) Minority heating. In this case we assume f = 38.5 MHz and a hydrogen concentration $n_h/n_d = 0.02$.
Figure (1) for Ant. I, and Fig. (2) for Ant. II show
$P_h(r) = \int_{-\pi}^{\pi} P_h(r,\theta)d\theta$, $P_d(r) = \int_{-\pi}^{\pi} P_d(r,\theta)d\theta$ and $P_e(r) = \int_{-\pi}^{\pi} P_e(r,\theta)d\theta$
for different values of the toroidal wave number $k_\phi = N/R$.
Here $P_h(r,\theta)$, $P_d(r,\theta)$ and $P_e(r,\theta)$ are the rf powers absorbed per unit volume by the minority ions via cyclotron damping, by the deuterium ions via second-harmonic cyclotron damping, and by the electrons via Landau damping, respectively. For each value of k_ϕ the corresponding value of ($Q = Im\{\int \vec{E}^* J^{ext} dV\}/Real\{\int \vec{E}^* J^{ext} dV\}$ is also given in the figure caption.
We emphasize here that P_e and P_d have been estimated in a non-self-consistent way; i.e. electron inertia and ion Larmor radius have been neglected throughout in the numerical evaluation and

P_e was evaluated from : $P_e = Real\{\int_{-\pi}^{\pi} J^*_{//} E_{//} d\theta\}$, by assuming
$|\frac{\partial^2 E_{//}}{\partial r^2}| << \frac{\Pi_e^2}{c^2} E_{//}$, so that $J_{//} \approx \frac{c^2}{4\pi\omega i} k_{//} (\frac{\partial E_r}{\partial r} + \frac{\partial E_\theta}{r\partial\theta})$ and $E_{//} = \frac{J_{//}}{\sigma_{//}}$.
Here $\sigma_{//} \approx 2\frac{\Pi_e^2}{c^2}\zeta_e^2\{1 + \zeta_e Z(\zeta_e)\}$, $Z(\zeta_e)$ is the plasma dispersion function and $\zeta_e = \frac{\omega}{|k_{//}|v_e}$;

P_d was evaluated from $P_d \approx \frac{1}{2}\rho_d^2 \sum_m (\frac{\partial E_m^+}{\partial r})^* \sum_n \sigma_{m.n}^{+d} \frac{\partial E_n^+}{\partial r}$,

where $\sigma_{m.n}^{+d} = \sigma_{m,n}^{+}$ after substituting $\frac{\Pi_d^2}{c^2}$ for $\frac{\Pi_h^2}{c^2}$ and v_d/Ω_h for ρ_h .

The asterisks indicate here complex conjugate.
All quantities are in arbitrary units, but the value of the current in the antenna has been kept constant throughout.
Figure (3) for Ant. I and Fig. (4) for Ant. II shows $P_h(r,\theta_n)$ and $|E^+(r,\theta_n)|$ as a function of the radius for different values of the poloidal angle: $\theta_n = -\frac{\pi}{2} + (n-1)\delta$, n = 1.... 16. To simplify the figure, the axes have been rotated by an angle: $-\theta_n$ for $-\frac{\pi}{2} \leq \theta_n \leq \frac{\pi}{2}$ and by an angle $\pi - \theta_n$ for $\frac{\pi}{2} \leq \theta_n \leq \frac{3\pi}{2}$.

Figure (5) a) and b) shows, in more detail, the same quantities as Figs. (3a) and (4a) respectively.
For low values of k_ϕ ($k_\phi \leq 0.05\ cm^{-1}$) ion-cyclotron damping is rather small so that a wave can approach a mode coversion layer:

$$\{k_{//}^2 + \frac{\Pi_d^2}{c^2}\frac{\omega^2}{\omega^2 - \Omega_d^2}\}E^+(r,\theta) + \sum_m e^{im\theta}\sum_n \sigma_{m,n}^+ E_n^+(r) \approx 0$$

practically undamped. On approaching a mode conversion layer, however, the perpendicular component of the group velocity decreases so that, in the absence of damping, the electric field of the wave would reach very large values. Moreover, propagating along the layer toward the ion-cyclotron resonance, the value of $|\frac{\partial E^+}{\partial \theta}|$ steadily increases so that a " magnetic beach effect ", as described by Stix /5/, can occur, in which case the values of both $|k_{//}| = |k_\phi + \frac{1}{qR}\frac{\partial}{\partial\theta}|$ and the electric field increases on approaching the resonance. The wave is, eventually, absorbed via ion-cyclotron damping. A competitive effect (which we have neglected here) is that terms proportional to $\rho_d^2|\frac{\partial^2 E^+}{\partial r^2}|$ become sufficiently large close to the mode conversion layer for a considerable fraction of the rf power to be absorbed by the majority ions after mode conversion.
For larger values of k_ϕ, ion cyclotron damping becomes more and more important so that the electric field remains finite at the mode conversion layer and the wave can cross the layer, reaching the plasma centre (minority heating).
If, however, the value of k_ϕ is too large ($k_\phi \geq 0.2\ cm^{-1}$), the wave can no longer propagate inside the plasma and the electromagnetic fields are only large close to the antenna. In this case the heating efficency becomes very low and, eventually, the value of Q resulting from resistive plasma loading becomes larger than the value due to ohmic losses in the antenna. In this case only a small fraction of the rf power coupled to the antenna contributes to the plasma heating. Moreover the largest part of this power is absorbed near the wall, where the plasma density is low and a few ions can be accelerated to very high energies.

b) Mode conversion. In this case we assume $f = 34.5\ MHz$ ($f_{ci} = 38.5\ MHz$) and $n_h/n_d = 0.15$ so that the ion-cyclotron resonance is outside the vacuum vessel $\Delta \approx 20\ cm$, while the two-ion hybrid resonance is inside the plasma volume $\Delta_h \approx -3\ cm$
Figure (7) to Fig. (8) show, for mode conversion heating, the same quantities as Figs. (1) to (2). Here we have assumed a collisional frequency $\nu/\omega \approx 2\ 10^{-4}$. Unlike for minority heating, the heating efficiency is now quite different for low-field-side coupling (Ant. I) and high-field-side coupling (Ant. II). In the low-field-side case, mode conversion is rather ineffective: the values of Q are quite large and depend on the value of the collisional frequency since mode conversion is weak. For the high-field-side antenna, on the other hand, the values of Q are comparable with those for minority heating and, at least for small values of k_ϕ ($k_\phi \leq 0.1\ cm^{-1}$), lower or comparable with the values of Q due to ohmic losses in the antenna.
For larger values of k_ϕ the mode conversion layer is shifted towards lower values of the

magnetic field and, eventually, moves outside the plasma volume.
The rf power absorbed by the electrons, P_e, were estimated in the same way as for minority heating. The rf power absorbed by the deuterium ions via second-harmonic ion-cyclotron damping is negligibly small and has been omitted from the figure.
From the numerical results it becomes clear that waves with large values of k_ϕ, ($k_\phi \geq .2\ cm^{-1}$), contribute very little to the resistive plasma loading of the antenna. These waves have very high Q values so that they only increase the reactive part of the antenna impedance and the value of the electromagnetic fields in the neighbourhood of the antenna. Waves with large values of k_ϕ tend, therefore, to accelerate particles, ions or electrons, in the vicinity of the wall, where the plasma density is low. They could, therefore, be the main cause of the impurity production observed in all ICRF heating experiments. On the other hand waves with low values of k_ϕ , ($k_\phi \leq 0.1\ cm^{-1}$) have an acceptable value of Q ($Q \leq 100$). so that an appreciable fraction of the rf power coupled to the antenna contributes to plasma heating.
We can therefore conclude that ICRF heating in the minority regime could still be feasible in the W VII-A stellarator provided that:
a) it is possible to design an antenna which couples a sufficently narrow k_ϕ spectrum around low values of k_ϕ; a non-trivial problem in the W VII-A stellarator since, if one wants to couple parallel wavelegths $\lambda_{//} \geq 40\ cm$, the antenna must necessarily be much broader than the diameter of the vacuum vessel ports ($\phi = 10\ cm$).
b) the hydrogen concentration can be kept sufficently low, $n_h/n_d \leq 2\ \%$; again non-trivial, since the hydrogen concentration due to recycling may be considerably larger than this limit.
An alternative possibility, in case the hydrogen concentration is too high and/or energetic ions must be avoided, could be electron Landau damping after mode conversion. Here again a sufficently narrow k_ϕ spectrum is required and the wave must be coupled, at least in part, from the high-magnetic-field side.

3. Antenna Design

Two antennas have been designed for the W VII-A stellarator:
Ant. I is a conventional antenna. It is fed at $\theta = \pi/4$ and short-circuited at $\theta = -\pi/4$. The width of the antenna is the same as that of the feeder so that the rf current on the antenna can be assumed to flow in the poloidal direction only. This antenna is rather narrow ($d = 6\ cm$) owing to the small diameter ($\phi = 10\ cm$) of the W VII-A ports and couples a quite broad spectrum of k_ϕ. This antenna is provided with a Faraday shield.
Ant. II is a broad antenna ($d = 75\ cm$). The antenna is fed at $\theta = \pi/4$ and short-circuited at $\theta = \pi$. Since the antenna is broader than the feeder, the rf current must have a toroidal component. The antenna has, however, slots in the poloidal direction so that the toroidal component of the rf current can only flow in a narrow strip around $\theta = \pi/4$. Since this antenna had to be introduced into the vacuum chamber in pieces through the small windows of the W VII-A stellarator, it was not possible to provide

the antenna with a Faraday shield without major technical complications. We decided, therefore, to short-circuit the antenna at both ends by two limiters, see Fig (9), and to perform the experiment without a Faraday shield. For the same reason the envisaged second half of the antenna (fed at $\theta = -\pi/4$ and short-circuited at $\theta = -\pi$) was not inserted.

The rf power coupled to the plasma will depend on the k_ϕ spectrum excited by the two antennas, which, in turn, is a function of the current distribution in the antennas. Owing to the small dimension of Ant. I, the current density can be assumed to be uniformly distributed on the antenna and on the feeder.

The situation is, however, much more complex for Ant. II. We can regard the strip where the toroidal current flows as a transmission line with a distributed series inductance L_o and a parallel admittance $Y = \omega C_o(1 - 1/\omega^2 L_1 C_o)$. The additional inductance L_1 in parallel to the capacitance C_o is due to the fact that a poloidal current can flow from the strip at $\theta = \pi/4$ to the short at $\theta = \pi$. If we now assume the current on the strip to vary as $I_\phi = I_o exp\{i(k_\phi z - \omega t)\}$, the value of L_1 will, in general, not only be a complicated function of the geometry of the system and of the plasma parameters but will also depend on k_ϕ itself so that k_ϕ will be determined by an equation of the form

$$k_\phi^2 = \omega^2 L_o C_o (1 - \frac{1}{\omega^2 L_1(k_\phi) C_o}) \tag{11}$$

In the W VII-A stellarator L_1 will be normally be rather small since the length of the antenna $l = 3s\pi/4$ is much shorter than $\lambda/4$ so that $k_\phi^2 < 0$ and I_ϕ will decay exponentially away from the feeder. However, if the plasma density is sufficently high and k_ϕ close to the value k_ϕ^* corresponding to a cavity resonance for the particular values of the plasma parameters,the real part of L_1 can assume, at least if the damping is small, quite large values (both positive and negative). It should therefore always be possible for a wave to propagate along the antenna with a value of k_ϕ close to k_ϕ^*. In this sense the antenna could be "self-tracking ". In the practical case of the W VII-A stellarator, however, the maximum value that $|L_1(k_\phi)|$ can reach in the presence of even a small amount of damping could, in order to satisfy eq.(11), be too low. On the other hand, if the damping is sufficiently small, eq(11) can be satisfied only by particular values of the plasma parameters since in this case the toroidal modes do not overlap. A self-consistent evaluation of the plasma-loaded antenna impedance and of the current distribution on the antenna is given in the next section.

4. Evaluation of the Antenna Impedance

We assume the antenna to consist of a thin conductor with a radius r = s, so that the antenna has a surface current which can have a poloidal $J_\theta^=$ and a toroidal $J_\phi^=$ component. The antenna is fed at $\theta = \theta_1$ and short-circuited at $\theta = \theta_2$. Both the current density in the feeder and in the short are assumed to flow in the radial direction from r = s to r = w where we assume a conducting wall. The current in the feeder is assumed to be driven by an e.m.f., and the distance between the antenna and the wall

to be sufficently small so that the current density can be assumed to be constant for $s \leq r \leq w$. The antenna can then be described by a diagonal conductivity tensor of the form

$$
\begin{aligned}
&\sigma_{\theta,\theta} = \sigma_o^{=} \cdot \delta(r-s) \cdot U(\theta, \theta_1 - \delta, \theta_2 + \delta) \cdot U(\phi, -\phi_o, \phi_o) \qquad \theta_1 < \theta_2 \\
&\sigma_{\phi,\phi} = \sigma_o^{=} \cdot \delta(r-s) \cdot U(\theta, \theta_1 - \delta, \theta_1 + \delta) \cdot U(\phi, -\phi_o, \phi_o) \\
&\sigma_{r,r} = \sigma_o \cdot \frac{s}{r} U(r, s, w) \cdot U(\theta, \theta_2 - \delta, \theta_2 + \delta) \cdot U(\phi, -\phi_o, \phi_o)
\end{aligned} \tag{10}
$$

where $l = s \cdot (\theta_2 - \theta_1)$ and $d = 2R\phi_o$ are the length and the width of the antenna, respectively, $d_s = 2s\delta$ is the poloidal width of the short and of the strip where the toroidal current can flow (which we assume for simplicity to be equal), σ_o is the conductivity of the short, and $\sigma_o^{=}$ is a surface conductivity, which we assume to be $\sigma_o^{=} = \sigma_o d_{sk}$, d_{sk} being the skin depth. The current density on the antenna can then be assumed to be of the form

$$
\vec{J}^{ext}(r,\theta,\phi) = \delta(r-s) \cdot \{\vec{e}_\theta \cdot J_\theta(\theta,\phi) + \vec{e}_z \cdot J_z(\theta,\phi)\} + \vec{e}_r \cdot \frac{s}{r} \cdot U(r,s,w) \cdot J_r(\theta,\phi) \tag{11}
$$

where $J_r(\theta,\phi) = \{J^s(\theta,\phi) + J^f(\theta,\phi)\}$, J^s , J^f being the current density in the short and feeder, respectively.
In order to evaluate the distribution of the rf currents on the antenna, we first evaluate the value of the electric field generated by a current distribution of the form given by eq. (2). The current distribution on the antenna can then be evaluated self-consistently as a function of the current density in the feeder from

$$
\vec{J}^{ext}(r,\theta,\phi) = \vec{\vec{\sigma}}(r,\theta,\phi) \cdot \vec{E}(r,\theta,\phi) + \vec{e}_r \cdot J^f(r,\theta,\phi) \tag{12}
$$

In order to evaluate the value of E and H for $r < p$, we simplify the problem by assuming the plasma density to be uniform for $r \leq p^*$ (p^* being the radius at which, for a given density profile, the wave has a cut-off, $k_o^2 - \sigma^-(r^*) = 0$) and the static magnetic field to be constant (we take into account the inhomogeneity of the static magnetic field roughly into account by averaging the local value of $k_\perp(r,\theta)$ over the plasma cross section). This is of course not correct if the mode conversion layer is inside the plasma volume. Here, however, we consider minority heating, $n_h << n_d$, and/or second-harmonic heating.
We perform Fourier analysis in θ and ϕ and obtain for $s \leq r \leq w$

$$
\begin{aligned}
H_m &= A^{(2)}_{m,n}\ a(r) + im \cdot J_r \cdot F(r) \\
E^\theta_m &= \frac{1}{k_o^2}\{A^{(2)}_m\ a'(r) + im \cdot J_r \cdot F'(r)\} \\
E^z_m &= B^{(2)}_m\ b(r)
\end{aligned} \tag{13}
$$

and for $p^* \leq r \leq s$

$$
\begin{aligned}
H_m &= A^{(1)}_{m,N}\{I_m(k_o r) + \nu K_m(k_o r)\} \\
E^{\theta}_m &= \frac{A^1_m}{k_o^2}\{I'_m(k_o r) + \nu K'_m(k_o r)\} \qquad (14) \\
E^{z}_m &= B^{(1)}_m \gamma_m(r)
\end{aligned}
$$

where

$$
\begin{aligned}
k_o &= k_\phi^2 - \frac{\omega^2}{c^2}, \qquad k_\phi = N/R, \\
H_m &= \frac{1}{r}\{(rE^{\theta}_m)' - im \cdot E^{r}_m\}, \\
a(r) &= K'_m(k_o w) I_m(k_o r) - I'_m(k_o w) K_m(k_o r), \qquad (15) \\
b(r) &= K_m(k_o w) I_m(k_o r) - I'_m(k_o w) K_m(k_o r), \\
F(r) &= I_m(k_o r) \int_w^r K_m(k_o x)dx - K_m(k_o r) \int_w^r I_m(k_o x)dx,
\end{aligned}
$$

and $\gamma_m(r) = K_m(k_o w_f) I_m(k_o r) - I_m(k_o w_f) K_m(k_o r)$ if a Faraday shield at $r = w_f$ is assumed. The primes here indicate derivatives with respect to r and $I_m(z)$, $K_m(z)$ denote Bessel functions in the notation of G.N. Watson.
In the limit $n_h/n_d \to 0$ and neglecting electron inertia, the local value of $k^2_\perp(r,\theta)$ is

$$
k^2_\perp(r,\theta) \approx k^2_{o\perp} + i\frac{\sqrt{\pi}}{2}\frac{(k_o^2 - \sigma_-^2)^2}{(k_o^2 - \sigma_1)^2} \cdot \{\frac{\Pi_h^2}{c^2}\frac{\omega}{k_{//} v_h} \cdot e^{-\varsigma_h^2} + \frac{\Pi_d^2}{c^2}\frac{k^2_{o\perp}\rho_d^2}{2}\frac{\omega}{k_{//} v_d} \cdot e^{-\varsigma_d^2}\} \qquad (16)
$$

so that for $\bar{k}_\perp = \frac{1}{\pi p^2}\int_{-\pi}^{\pi} d\theta \int_0^p k_\perp(r,\theta) r dr$ one has

$$
\bar{k}_\perp \approx k^2_{o\perp} + i\frac{R}{2p}\frac{(k_o^2 - \sigma_-)^2}{(k_o^2 - \sigma_1)}\{\frac{\Pi_h^2}{c^2} + \frac{1}{2}\frac{\Pi_d^2}{c^2} k^2_{o\perp}\rho_d^2\} \qquad (17)
$$

where

$$
\begin{aligned}
k^2_{o\perp} &= (k_0^2 - \sigma_-)\{2 - \frac{k_o^2 - \sigma_-}{k_o^2 - \sigma_1}\} \\
\sigma^- &= \frac{\Pi_d^2}{c^2}\frac{\omega^2}{\Omega_d(\omega + \Omega_d)} \qquad (18) \\
\sigma_1 &= -\frac{\Pi_d^2}{c^2}\frac{\omega^2}{\omega^2 - \Omega_d^2} \\
\varsigma_h &= \frac{r\omega cos\theta}{Rk_{//} v_h}, \quad \varsigma_d = \frac{r\omega cos\theta}{Rk_{//} v_d}
\end{aligned}
$$

Under these assumptions we then have, for $r \leq p^*$

$$
\begin{aligned}
H_m &= A_m^o \; J_m(\bar{k}_\perp r) \\
E_m^\theta &= \frac{A_m^o}{k_\perp^2}\{J_m'(\bar{k}_\perp r) + \frac{\sigma_- - \sigma_1}{k_o^2 - \sigma_1} J_m(\bar{k}_\perp r)\} \\
E_m^z &= 0
\end{aligned} \tag{19}
$$

The constants A,B, ν can now be determined by the boundary conditions at $r = p^*$ and $r = s$:

$$
\begin{aligned}
&\{H_m\}_{p^*} = 0 \qquad \{E_m^\theta\}_{p^*} = 0 \\
&\{H_m\}_s = -\frac{4\pi i\omega}{c^2} J_m^\theta \qquad \{E_m^\theta\}_s = 0 \\
&\{E_m^\phi\}_s = 0 \qquad \{\frac{dE_m^\phi}{dr}\}_s = \frac{4i\pi}{\omega}\{\frac{k_z m}{r} J_m^\theta + k_o^2 J_m^z - ik_z J_m^r\}
\end{aligned} \tag{20}
$$

where $\{E\}_x = \frac{lim}{\delta \to 0}(E(x+\delta) - E(x-\delta))$.

From eqs (7), (8) we obtain the value of the electric field in the form

$$
\vec{E}(r,\theta,\phi) = \sum_N \sum_m \vec{\chi}_{N,m}(r) \cdot \vec{J}_{N,m} e^{im\theta} e^{iN\phi} \tag{21}
$$

The components of $\vec{\chi}_{N,m}$ are given by

$$
\begin{aligned}
\chi_{N,m}^{\theta,\theta}(s) &= -\frac{1}{k_o^2}\{\frac{1}{D_a} + \frac{m^2 k_\phi^2 c^2}{s^2\omega^2 D_b}\} \\
\chi_{N,m}^{\theta,\phi}(s) &= -\frac{c^2}{\omega^2}\frac{mk_\phi}{sD_b} \\
\chi_{N,m}^{\theta,r}(s) &= i\frac{m}{k_o^2}\{\frac{-\alpha}{D_a} - \frac{k_\phi^2 c^2}{s\omega^2 D_b}\} \\
\chi_{N,m}^{\phi,\theta}(s) &= -\frac{c^2}{\omega^2}\frac{mk_\phi}{sD_b} \\
\chi_{N,m}^{\phi,\phi}(s) &= -\frac{c^2}{\omega^2}\frac{k_o^2}{D_b} \\
\chi_{N,m}^{\phi,r}(s) &= i\frac{c^2}{\omega^2}\frac{k_\phi}{D_b} \\
< \chi_{N,m}^{r,\theta} > &= i\frac{m}{k_o^2}\{\frac{H}{D_a} + \frac{k_\phi^2 c^2}{s\omega^2 D_b}\} \\
< \chi_{N,m}^{r,\phi} > &= i\frac{c^2}{\omega^2}\frac{k_\phi}{D_b} \\
< \chi_{N,m}^{r,r} > &= \frac{1}{k_o^2}\{m^2\frac{-\alpha H}{D_a} + \frac{k_\phi^2 c^2}{\omega^2 D_b} - m^2 K - (w-s)\}
\end{aligned} \tag{22}
$$

where

$$D_a = \frac{a(s)}{a'(s)} - \frac{I_m(k_o s) + \nu K_m(k_o s)}{I'_m(k_o s) + \nu K'(k_o s)}$$

$$D_b = -\frac{b(s)}{b'(s)} + \frac{\gamma'(s)}{\gamma(s)}$$

$$\nu = -\frac{I'_m(k_o p) + \mu I_m(k_o p)}{K'_m(k_o p) + \mu K_m(k_o p)}$$

$$\mu = -\frac{k_o^2}{k_\perp^2}\{\frac{J'_m(\bar{k}_\perp p^*)}{J_m(\bar{k}_\perp p^*)} + \frac{\sigma_- - \sigma_1}{k_o^2 - \sigma_1}\} \tag{23}$$

$$\alpha = F(s) - F'(s)\frac{a(s)}{a'(s)}$$

$$H = \frac{1}{a'(s)} \int_w^s a(r)dr$$

$$K = F'(s)H - \int_w^s \frac{F(r)}{r}dr$$

It is now convenient to write the current density on the antenna in the form

$$\vec{J}^{ext}(r,\theta,\phi) = \frac{\vec{\sigma}(r,\theta,\phi)}{\sigma_o} \cdot \vec{J}^*(\theta,\phi) + \vec{e}_r J^f(r,\theta,\phi) \tag{24}$$

where:

$$J^{*\theta}(\theta,\phi) = \sum_M \sum_n J^{*\theta}_{M,n} e^{in\alpha\theta} e^{iM\beta\phi}$$

$$J^{*\phi}(\theta,\phi) = \sum_m \sum_n J^{*\phi}_{M,n} e^{in\alpha_o\theta} e^{iM\beta\phi} \tag{25}$$

$$J^{*s}(\theta,\phi) = \sum_m \sum_n J^{*s}_{M,n} e^{in\alpha_o\theta} e^{iM\beta\phi}$$

where $\alpha \leq 2\pi/|\theta_2 - \theta_1 + 2\delta|$, $\alpha_o \leq \pi/\delta$ and $\beta \leq \pi/\Phi_o$.
We now simplify the problem by neglecting the ohmic losses in the short so that $\int_s^w \sigma_{r,r}(r,\theta,\phi)E^r(r,\theta,\phi)dr = 0$, and by assuming $2s\delta$ to be sufficiently small so that the toroidal component of the surface current and the current density in the feeder can be assumed to be constant for $\theta_1 - \delta \leq \theta \leq \theta_1 + \delta$ and the current density in the short to be constant for $\theta_2 - \delta \leq \theta \leq \theta_2 + \delta$ i.e. $J^{\phi}_{M,n} \approx J^{*\phi}_M \ \delta_{n,0}$ and $J^s_{M,n} \approx J^{*s}_M \ \delta_{n,0}$, $\delta_{m,n}$ being the Kroenecker symbol .
From eqs. (4), (5) we then have

$$\sum_M \sum_n T^{\theta,\theta}_{\bar{M},M,\bar{n},n} J^{*\theta}_{M,n} + \sum_M T^{\theta,\phi}_{\bar{M},M,\bar{n}} J^{*\phi}_M + \sum_M T^{\theta,r}_{\bar{M},M,\bar{n}} J^{*s}_M = \Gamma^{\theta}_{\bar{M},\bar{n}}$$

$$\sum_M \sum_n T^{\phi,\theta}_{\bar{M},M,n} J^{*\theta}_{M,n} + \sum_M T^{\phi,\phi}_{\bar{M},M,} J^{*\phi}_M + \sum_M T^{\phi,r}_{\bar{M},M} J^{*s}_M = \Gamma^{\phi}_{\bar{M}} \tag{26}$$

$$\sum_M \sum_n T^{r,\theta}_{\bar{M},M,n} J^{*\theta}_{M,n} + \sum_M T^{r,\phi}_{\bar{M},M} J^{*\phi}_M + \sum_M T^{r,r}_{\bar{M},M} J^{*s}_M = \Gamma^{r}_{\bar{M}}$$

where

$$T^{\theta,\theta}_{\bar{n},n\bar{M},M} = \sum_N \sum_m \chi^{\theta,\theta}_{N,m}(s) F^m_n F^m_{\bar{n}} S^N_{M,\bar{M}}$$

$$T^{\theta,\phi}_{\bar{n},\bar{M},M} = \sum_N \sum_m \chi^{\theta,\phi}_{N,m}(s) F^m_{\bar{n}} \gamma^{(2)}_m S^N_{M,\bar{M}}$$

$$T^{\theta,r}_{\bar{n},\bar{M},M} = \sum_N \sum_m \chi^{\theta,r}_{N,m}(s) F^m_{\bar{n}} \gamma^{(1)}_m S^N_{M,\bar{M}}$$

$$T^{\phi,\theta}_{n,\bar{M},M} = \sum_N \sum_m \chi^{\phi,\theta}_{N,m}(s) F^m_n \gamma^{(1)}_m S^N_{M,\bar{M}}$$

$$T^{\phi,\phi}_{\bar{M},M} = \sum_N \sum_m \chi^{\theta,r}_{N,m}(s) \gamma^{(2)}_m \gamma^{(1)}_m S^N_{M,\bar{M}} \qquad (27)$$

$$T^{\phi,r}_{\bar{M},M} = \sum_N \sum_m \chi^{\phi,r}_{N,m}(s) \gamma^{(1)}_m \gamma^{(1)}_m S^N_{M,\bar{M}}$$

$$T^{r,\theta}_{n,\bar{M},M} = \sum_N \sum_m < \chi^{r,\theta}_{N,m} > F^m_n \gamma^{(2)}_m S^N_{M,\bar{M}}$$

$$T^{r,\phi}_{\bar{M},M} = \sum_N \sum_m < \chi^{r,\phi}_{N,m} > \gamma^{(2)}_m \gamma^{(2)}_m S^N_{M,\bar{M}}$$

$$T^{r,r}_{\bar{M},M} = \sum_N \sum_m < \chi^{r,r}_{N,m} > \gamma^{(1)}_m \gamma^{(2)}_m S^N_{M,\bar{M}}$$

$$\Gamma^{\theta}_{\bar{M}} = -\sum_N \sum_m J^f_N \chi^{\theta,r}_{N,m} F^m_{\bar{n}} \gamma^{(2)}_m S^N_{\bar{M}}$$

$$\Gamma^{\phi}_{\bar{M}} = -\sum_N \sum_m J^f_N \chi^{\phi,r}_{N,m} \gamma^{(2)}_m \gamma^{(1)}_m S^N_{\bar{M}} \qquad (28)$$

$$\Gamma^{r}_{\bar{M}} = -\sum_N \sum_m J^f_N < \chi^{r,r}_{N,m} > \gamma^{(2)}_m \gamma^{(2)}_m S^N_{\bar{M}}$$

and where

$$< \chi_{N,m} > = \int_w^s \chi_{N,m}(r)\, dr,$$

$$S^N_{M,\bar{M}} = S^N_M \cdot S^N_{\bar{M}} \qquad S^N_{\bar{M}} = \frac{sin(N-\beta\bar{M})\Phi_o}{N-\beta\bar{M}} \qquad (29)$$

$$F^m_n = \frac{sin(m-n\alpha)\theta}{m-n\alpha},$$

$$\gamma^{(1)}_m = \frac{sin(m\delta)}{m\delta}\, e^{-im\theta_2}, \qquad \gamma^{(2)}_m = \frac{sin(m\delta)}{m\delta}\, e^{-im\theta_1}$$

Eq(17) has been solved numerically and the antenna impedance Z has been evaluated from ($Z = \{\int E^*_r \cdot J^f dV\}/\{\int |J^f|^2 dV\}$.

Figure (10) shows as a function of the plasma line density:
a) for Ant. I and b) for Ant. II the evaluated value of the resistive plasma loading;
c) for Ant. I and d) for Ant. II the corresponding value of Q (solid curve) and the maximum value of the rf power P (dotted curve), which can be coupled to the plasma if the ohmic losses in the antenna and in the transmission line are neglected and the voltage at the antenna is assumed to be $V = 20\ kV$. The left scale refers to the values of Q and the right scale to the values of P (kW);
e) the k_ϕ spectrum coupled by Ant. I and f) the k_ϕ spectrum coupled by Ant. II.
A parabolic density profile and the following values of the plasma parameters were assumed: major radius R = 200 cm, antenna radius s = 14 cm, plasma radius p = 6 cm, ion temperature $T_i = 400$ eV and hydrogen concentration $n_h/n_d = 0.02$. Since, in absence of plasma, the resistive loading of Ant. II due to ohmic losses in the antenna and in the the trasmission line is of the order of 0.3 ohms, the rf power coupled to the plasma could be as large as 50 % of the total power coupled to the antenna. Unfortunately, such high efficiencies are only predicted for values of the plasma density which are beyond the values which can be reached by ECRF heating alone. For lower densities the value of Q decreases quite rapidly so that for the standard values of the line density $\bar{n} \cdot L \leq 4.5\ 10^{14} cm^{-2}$ no more than 10 to 20 % of the total rf power coupled to the antenna can be expected to be absorbed by the plasma.
The values of Q evaluated for Ant. I are, on the other hand, far too high so that a very low amount of rf power can be coupled to the plasma for acceptable values of the voltage at the antenna. This kind of antenna is, however, much simpler than Ant. II, it can be inserted (and removed) through the vacuum vessel ports of the W VII-A stellarator and can easily be provided with a Faraday shield. For all these reasons Ant. I has been inserted in the W VII-A stellarator in spite of the bad heating efficency predicted by the theory.
The dotted curve in fig. b) shows the experimental value of the resistive plasma loading of Ant. II measured at very low rf power during the decay of the plasma density. In this case the plasma was generated by ECRF heating and sustained by neutral injection so that the value of the plasma density could be increased beyond the-cut off of the ECRF. The maximum value of the evaluated resistive plasma loading is shifted toward lower values of the plasma density and is broader than the measured one. The discrepancies between the evaluated and measured values of the resistive plasma loading are, however, not too surprising in view of the rough approximations made in the theoretical evaluations and of the uncertainity in the actual value of such parameters as plasma density profile or hydrogen concentration. Note that a much better fitting of the experimental values can be reached by choosing a smaller value of the plasma radius (i.e. a more peaked density profile), in which case the maximum value of the resistive plasma loading would shift to higher values of the line density, and by decreasing (or greatly increasing, i.e. $n_h/n_d >> p/R$) the value of the hydrogen concentration, thus narrowing the profile of the resistive plasma loading.

5. Experimental Results

Ion cyclotron heating was applied in the W VII-A stellarator in a current-free ECRF heated target plasma. Different heating mechanism have been investigated as minority heating, second-harmonic heating and electron Landau damping via mode conversion. The rf power ranged up to $P = 250\ kW$ at frequencies between $f = 34\ MHz$ and $f = 78\ MHz$.

Minority heating. Minority heating was attempted in an ECRF heated deuterium plasma with a minority of hydrogen ions. The magnetic field strength was kept constant at a value B= 2.53 T corresponding to the electron cyclotron resonance for the gyratron frequency ($f = 70\ GHz$). In order to have both the two-ion hybrid resonance and the ion cyclotron resonance inside the plasma volume, the hydrogen concentration has to be very low ($n_h/n_d \leq 3\ \%$) owing to the large aspect ratio ($A \approx 20$) of the W VII-A stellarator. We started the experiment with no hydrogen added in the gas feed. At a later time about 2 % hydrogen was added. No significant difference could be observed between the two situations. It is probable that the hydrogen concentration due to recycling was already considerably larger than 2 %.
The experiment was started with Ant. I. The maximum rf power coupled to the antenna was, however, limited to $P \leq 50\ kW$ owing to arcing in the transmission line. This is consistent with the theory, which predicts very high Q values for this kind of antenna. No significant changes could be observed in the plasma parameters for such low rf power.
The experiment continued with Ant. II . The net rf power coupled to this antenna could be raised up to $P = 250\ kW$.
At the start of the rf pulse the total plasma energy content increased by $\Delta E \approx 80\ J$ in a time $\tau \approx 2\ to\ 3\ ms$ and remained practically constant for a time $\tau \approx 10\ ms$. During this time the line density increased by about 10 % and the electron temperature (from soft X-ray and ECR emission) significantly decreased: $\Delta T_e \approx -300\ eV$
The bolometric signal more than doubled during the rf pulse with an increase in the radiated power : $P_{rad} \geq 40\ kW$; see Fig. (11). Badly confined energetic CX ions were observed during the rf pulse. The decay time of the energetic ions was $\tau \leq 2\ ms$. The energetic ions form a tail in the energy distribution with a temperature $T_h \approx 2\ keV$, as compared with a bulk ion tenperature $T_i \approx 400\ eV$.
During the first few milliseconds an rf power $P \approx 25\ to\ 40\ kW$ is absorbed by the plasma with a heating efficency : $\eta \approx 10\ to\ 15\ \%$.
For longer rf pulses, $\tau > 10$ ms, the total energy content decreased almost linearly during the remainder of the rf pulses and continued to decrease, more rapidly, after the end of the rf pulse. The line density increased during the rf pulse and the electron temperature decreased quite rapidly: typically from $\bar{n} \cdot L \approx 4\ 10^{14}\ cm^{-2}$ to $\bar{n} \cdot L \approx 5\ 10^{14}\ cm^{-2}$ and from $T_e \approx 1.5\ keV$ to $T_e \approx 500\ eV$ for an rf power $P = 250\ kW$ coupled to the antenna and a pulse duration $\tau = 20\ ms$.
The drastic decrease in the plasma energy content for longer rf pulses can be attributed

both to enhanced radiative losses due to the increase in the impurity content and to the fact that the plasma density increases and, eventually, reaches values close to the cut-off for the ECRF wave ($n_e \approx 6\ 10^{13}\ cm^{-3}$), thus strongly reducing the ECRF heating efficency in the central region and causing the observed strong electron cooling.

Mode conversion. Although the main cause of impurity production is not clear, a possibile source could be that energetic ions created in the vicinity of the antenna strike the wall. It must be remembered here that, in the minority heating regime, Ant. II crosses the ion-cyclotron layer so that, although the toroidal drift points towards the core of the plasma at the antenna position, energetic ions created in the vicinity of the antenna are, nevertheless, very badly confined in the small-dimension W VII-A plasma. For this reason an attempt has been done to avoid energetic ions and to heat electrons via mode conversion . For this purpose the wave frequency was lowered to $f = 33.5\ Mhz$ so that the ion cyclotron resonance was well outside the vacuum vessel of the W VII-A stellarator . At the same time the hydrogen concentration has been increased to $n_h/n_d \approx 20\ \%$ in order to have the two-ion hybrid resonance close to the plasma centre. No energetic ions should be generated in this situation. Nevertheless the increase in the radiative losses were comparable with those of minority heating. The total plasma energy content decreased (apart from a small increase during the first few milliseconds) almost linearly during the rf pulse.
The heating efficency was, in this case, very low and no effective electron heating could be observed. This is, at first, in contradiction with the theory, which predicts electron heating and an efficiency comparable, at least if k_ϕ is sufficently small, with that of minority heating. It must be emphasised, however, that, owing to the large aspect ratio of the W VII-A stellarator, the heating efficiency of mode conversion is very sensitive to the value of the hydrogen concentration so that even a small change of a few per cent in the hydrogen concentration can shift the mode conversion layer to the plasma border, thus considerably lowering the heating efficiency. Since no energetic CX ions were observed during the experiment a cause of the impurity production could be, in this case, paricles accelerated by the high electric fields in the vicinity of the antenna. It is recalled here that in Ant. II the parallel electric fields are not shielded.

Second-harmonic heating. The experiment continued with a plasma generated by ECRF heating and sustained by neutral injection. In this case the plasma density could be increased well beyond the cut-off of the ECRF wave and could reach values for which " cavity resonances " could play an important role.
Since a hydrogen beam was injected into a deuterium plasma, the hydrogen concentration was both too high and too badly defined for minority heating or for mode conversion heating to be effective. We therefore decided to work at the second harmonic of the hot hydrogen ions $f = 77\ MHz$. During the experiment the polarity of the current in the helical windings was inverted so that the experiment started with the plasma ellipse in the horizontal position and continued with the ellipse in the vertical position, i.e. closer to the antenna.
Here again a quite ineffective plasma heating is overshadowed by a large increase of the

radiation losses. The increase in the radiative losses is much larger with the plasma ellipse in the vertical position, i.e. closer to the antenna, than with the plasma ellipse in the horizontal position: $P_{rad} \approx 150\ kW$ and $P_{rad} \approx 50\ kW$, respectively, for a rf power P = 250 kW coupled to the antenna compared with discharges without rf, the total energy content decreases at the rates $\frac{dE}{dt} \approx -50\ kW$ and $\frac{dE}{dt} \approx -20\ kW$; respectively see Figs. (13) and (14), respectively.
The strong dependence of the radiative losses on the distance between the plasma and the antenna suggests that the main cause of the impurity production is that particles, ions or electrons accelerated in the high fields in the vicinity of the antenna strike the wall or the antenna itself. Unfortunately the W VII-A experiment was shut down before it was possible to provide Ant. II with a Faraday shield, so that it remains an open question whether and to what extent the parallel electric fields, which are not shielded in this kind of antenna, are responsible for the impurity production.

6. Discussion

Detailed analysis of wave propagation and rf power absorption in the W VII-A plasma has shown that, in spite of its small dimensions, ICRF heating could be feasibile in the W VII-A stellarator provided that certain conditions on the plasma parameters could be fulfilled, e.g. in the minority heating regime, the hydrogen concentration could be kept sufficently low, ($\eta \leq 2\%$). It has also been shown that only a narrow portion of the k_ϕ spectrum ($|k_\phi| \leq 0.1\ cm^{-1}$) effectively contributes to the plasma heating. A self-consistent numerical analysis of the plasma loaded impedance of the two antennas inserted in the W VII-A stellarator has shown that, for an acceptable voltage at the antenna ($V \leq 20\ kV$), only a limited amount of rf power ($P \leq 20\ kW$) can be coupled to the plasma by the conventional antenna while, at least for sufficently high values of the plasma density and if the ohmic losses are neglected, up to a few megawatts could, theoretically, be coupled by the broad antenna Not more than 50 kW of rf power could be coupled, becouse of arcing in the trasmission line, to the conventinal antenna as compared with a rf power $P \geq 250\ kW$ coupled to the broad antenna. This confirms, at least qualitatively, the numerical results. The heating efficency was, however, rather low $\eta \leq 15\ \%$. This is still in agreement with the theoretical evaluation which predicts, for such low values of the plasma line density, as could be attained by ECRF heating ($n \cdot L \leq 4.5 \cdot 10^{14}\ cm^{-2}$), that the resistive plasma loading of the antenna is only a small fraction of the resistive loading due to ohmic losses in the trasmission line and in the antenna itself. A more quantitative comparison with the theoretical results is not, however, possible since more or less effective plasma heating was always overshadowed by a large increase in the radiative losses. The main cause of radiative losses is not clear. In the minority heating regime badly confined high-energy ions generated in the vicinity of the antenna could be the main cause of impurity production. The radiation losses in the mode conversion heating regime were, however, comparable with those of minority heating although no high-energy ions were observed. A possible cause of impurity production could be, in this case, electrons accelerated by the parallel electric fields in the low density plasma close to the antenna. It must be remembered here that

the broad antenna had no Faraday shield. Unfortunately it is not possible to compare the impurity production of the broad antenna with that of the conventional antenna, which is provided with a Faraday shield, since the maximum rf power which could be coupled to this antenna was too low in order to see any significant change in the plasma parameters.

Figure captions :

Fig. (1): Ant. I: rf power absorbed per unit volume (averaged over the poloidal angle) by the hydrogen ions P_h (solid curve), by the deuterium ions P_d (dotted curve) and by electrons P_e (dot-dashed curve) versus radius for different values of k_ϕ. The assumed density profile is given in Fig. (6), the wave frequency is f = 38.5 MHz (f = f_{ch}), the ion temperature is $T_i = T_e = 400\ eV$ and the hydrogen concentration is n_h/n_d =0.02. The units are arbitrary, but the absolute value of the current density in the antenna has been kept constant throughout.

Fig. (2): Ant. II: Same quantities as in Fig(1).

Fig. (3): Ant. I: rf power $P(r,\theta)$ absorbed by the hydrogen ions per unit volume and $|E^+(r,\theta)|$ as a function of radius for the same value of the plasma parameters as in Fig. (1) and different values of the poloidal angle, $\theta_n = -\frac{\pi}{2} + (n-1)\delta$, n = 1.... 16. To simplify the figure, the axes have been rotated by an angle $-\theta_n$ for $-\frac{\pi}{2} \leq \theta_n \leq \frac{\pi}{2}$ and by an angle $\pi - \theta_n$ for $\frac{\pi}{2} \leq \theta_n \leq \frac{3\pi}{2}$. The units are again arbitrary the maximum value of the rf power P^{max} and of the electric field E^{max} being given in the footnote of the figure caption.

Fig. (4): Ant. II: Same quantities as in Fig(3).

Fig. (5): a) Same quantities as in Fig(3a) and b) in Fig(4a), in more detail.

Fig. (6): Density profile.

Fig. (7): Ant. I: rf power absorbed per unit volume (averaged over the poloidal angle) (solid curve), and rf power absorbed by electrons P_e (dotted curve), versus radius for different values of k_ϕ. The assumed density profile is given in Fig. (6), the wave frequency is f = 33.5 MHz ($f < f_{ch}$), the collisional frequency is $\nu = 2\ 10^{-4} \cdot f$ and the hydrogen concentrtion is $n_h/n_d = 0.15$.

Fig. (8): Ant. II: Same quantities as in Fig (7).

Fig. (9): Photo of the two antennas.

Fig. (10): a) Evaluated value of the resistive plasma loading of Ant. I and b) of Ant. II,
c) Evaluated value of Q (solid curve, left scale) and of the maximum rf power coupled to the plasma (dotted curve, right scale) by Ant. I and d) by Ant. II; the ohmic losses in the antenna are neglected here and the voltage at the antenna is assumed to be $V = 20\ kV$.
e) Evaluated k_ϕ spectrum coupled by Ant. I and f) by Ant. II;
the dotted curve in Fig. b) is the value of the resistive plasma loading measured at very low rf power during the decay of the plasma density.

Fig. (11): shows for minority heating with Ant. II
a) line density (cm^{-2}), b) total plasma energy content (kJ),
c) soft X-ray electron temperature (keV), d) total radiated power (kW),
e) rf power (kW); with rf (solid) and without rf (dotted).
The wave frequncy is f = 38.5 MHz ($f = f_{ch}$) and the hydrogen concentration in the gas feed is $n_h/n_d = 0.02$.

Fig. (12): shows for mode conversion with Ant. II the same quantities as in Fig(11).
The wave frequency is here f = 34.5 MHz ($f < f_{ch}$) and the hydrogen concentration in the gas feed is $n_h/n_d = 0.2$

Fig. (13): shows for second harmonic heating with Ant. II the same quantities as in Fig(11). The wave frequency is here f = 77 MHz ($f = 2 \cdot f_{ch}$) and the plasma ellipse is in the horizontal position.

Fig. (14): shows for second harmonic heating with Ant. II the same quantities as in Fig. (13). The wave frequency is again f = 77 MHz ($f = 2 \cdot f_{ch}$) and the plasma ellipse is in the vertical position.

References

1) J. ADAM et al. 5^{th} Conf. Pl. Phys. and Nucl. Fusion Res. (Tokyo 1974) II, 65, (1975).
2) V.L. VDOVIN, V.D. RUSANOV, N.V. SHAPOTKOVSKI, ibid. I, 217, (1975).
3) N.V. IVANOV , I.A. KOVAN , V.S. SVISHCHEV, JEPT Lett. 20, 39 , (1974) .
4) G. CATTANEI, Report IPP 2/272 1984
5) T.H. STIX, Theory of Plasma Waves (McGraw-Hill, New-York, 1962)

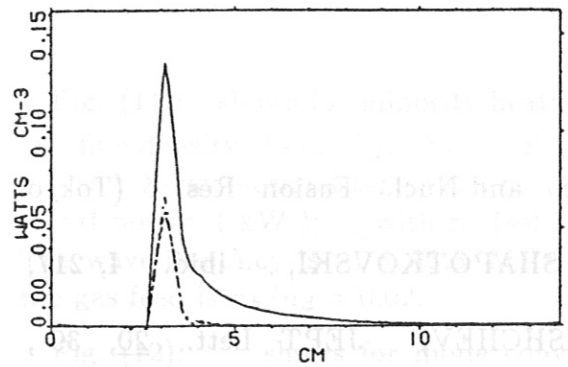

Fig(1) Ant.I a) $k_\phi = 0.$,

f = 38.5 MHz, $\nu = 0.$, Q = 16.8

P_h (solid) $P_d \cdot 10^{-1}$ (- - -) ; $P_r \cdot 10^{1}$ (— · —)

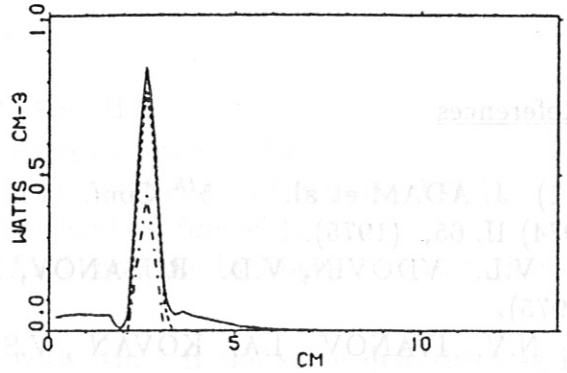

b) $k_\phi = 0.05$ cm^{-1},

f = 38.5 MHz, $\nu = 0.$, Q = 7.53

P_h (solid) $P_d \cdot 10^{-1}$ (- - -) ; P_r (— · —)

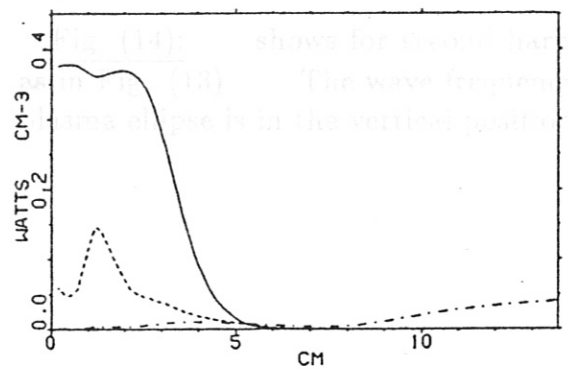

c) $k_\phi = 0.10$ cm^{-1},

f = 38.5 MHz, $\nu = 0.$, Q = $2.42 \cdot 10^2$

$P_h \cdot 10^{1}$ (solid) $P_d \cdot 10^{2}$ (- - -) ; $P_r \cdot 10^{3}$ (— · —)

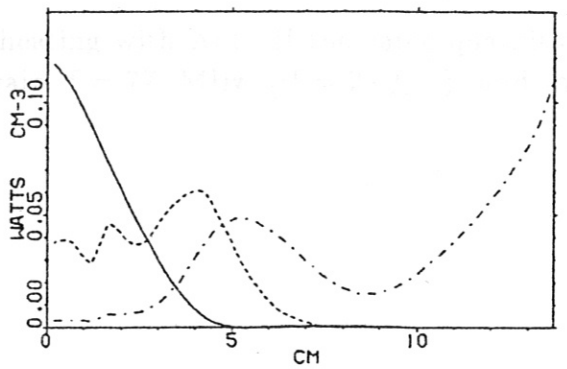

d) $k_\phi = 0.15$ cm^{-1},

f = 38.5 MHz, $\nu = 0.$, Q = $5.91 \cdot 10^2$

P_h (solid) $P_d \cdot 10^{2}$ (- - -) ; $P_r \cdot 10^{3}$ (— · —)

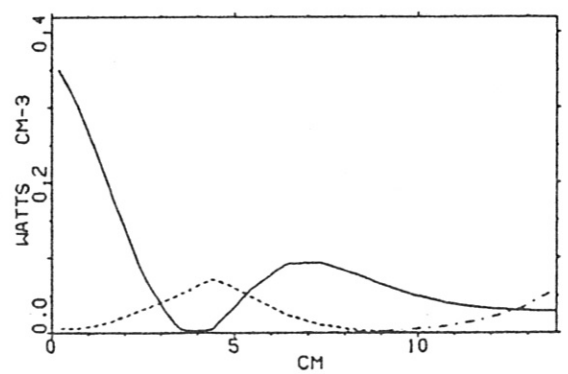

e) $k_\phi = 0.20$ cm^{-1},

f = 38.5 MHz, $\nu = 0.$, Q = $1.35 \cdot 10^4$

$P_h \cdot 10^{3}$ (solid) $P_d \cdot 10^{4}$ (- - -) ; $P_e \cdot 10^{2}$ (— · —)

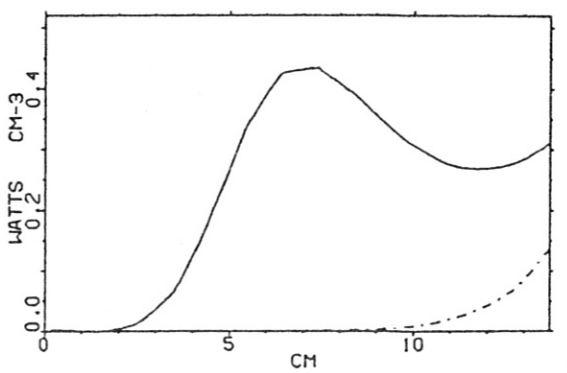

f) $k_\phi = 0.25$ cm^{-1},

f = 38.5 MHz, $\nu = 0.$, Q = $1.62 \cdot 10^4$

$P_h \cdot 10^{4}$ (solid) $P_d \cdot 10^{5}$ (- - -) ; $P_e \cdot 10^{2}$ (— · —)

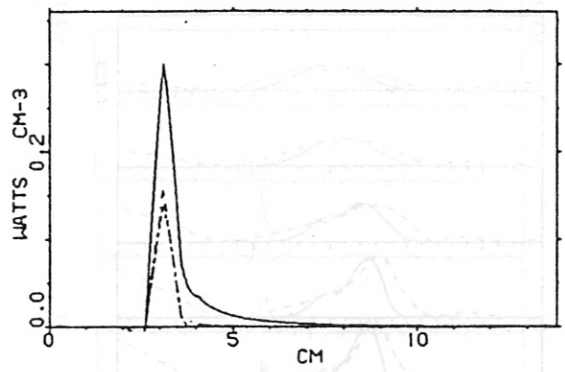

Fig(2) Ant.II a) $k_\phi = 0$

f = 38.5 MHz, $\nu = 0.$, Q = 17.0

P_h (solid) ; $P_d \cdot 10^{-1}$ (- - -) ; $P_e \cdot 10^{1}$ (— · —)

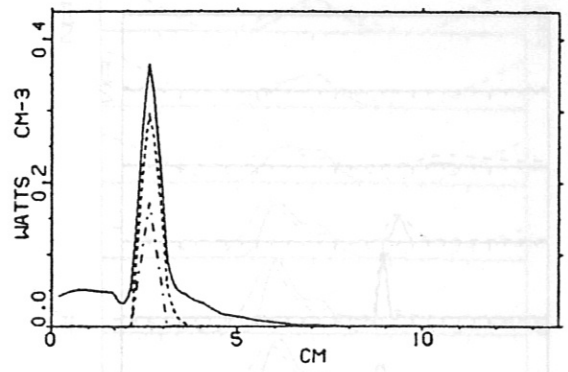

b) $k_\phi = 0.05\ \mathrm{cm}^{-1}$,

f = 38.5 MHz, $\nu = 0.$, Q = 33.3

P_h (solid) ; $P_d \cdot 10^{-1}$ (- - -) ; P_e (— · —)

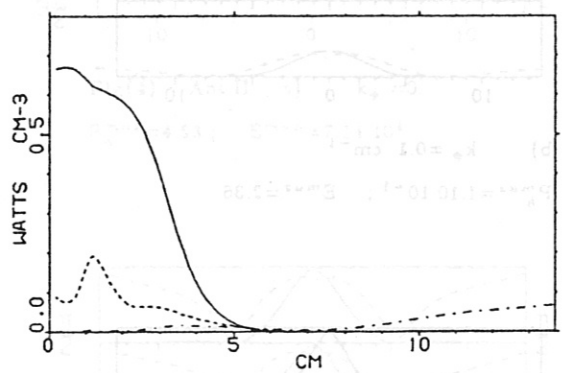

c) $k_\phi = 0.10\ \mathrm{cm}^{-1}$,

f = 38.5 MHz, $\nu = 0.$, Q = $2.87 \cdot 10^2$

$P_h \cdot 10^1$ (solid) ; $P_d \cdot 10^2$ (- - -) ; $P_e \cdot 10^3$ (— · —)

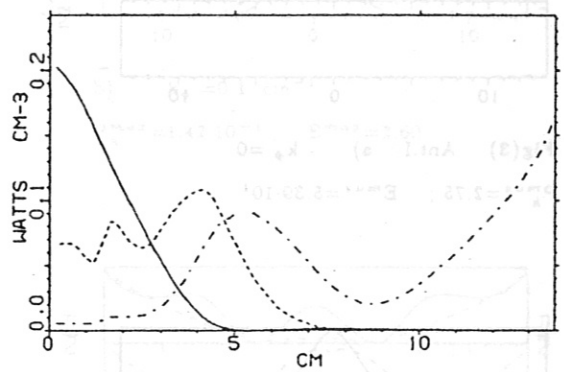

d) $k_\phi = 0.15\ \mathrm{cm}^{-1}$,

f = 38.5 MHz, $\nu = 0.$, Q = $9.35 \cdot 10^2$

P_h (solid) ; $P_d \cdot 10^2$ (- - -) ; $P_e \cdot 10^3$ (— · —)

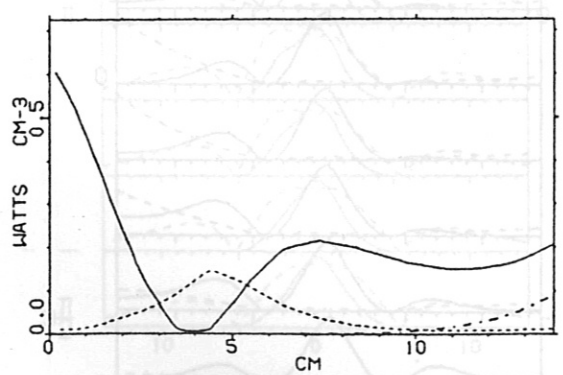

e) $k_\phi = 0.20\ \mathrm{cm}^{-1}$,

f = 38.5 MHz, $\nu = 0.$, Q = $3.27 \cdot 10^3$

$P_h \cdot 10^3$ (solid) ; $P_d \cdot 10^4$ (- - -) ; $P_e \cdot 10^2$ (— · —)

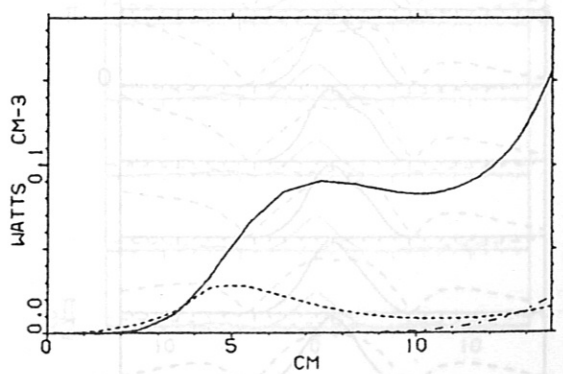

f) $k_\phi = 0.25\ \mathrm{cm}^{-1}$,

f = 38.5 MHz, $\nu = 0.$, Q = $4.49 \cdot 10^3$

$P_h \cdot 10^3$ (solid) ; $P_d \cdot 10^4$ (- - -) ; $P_e \cdot 10^1$ (— · —)

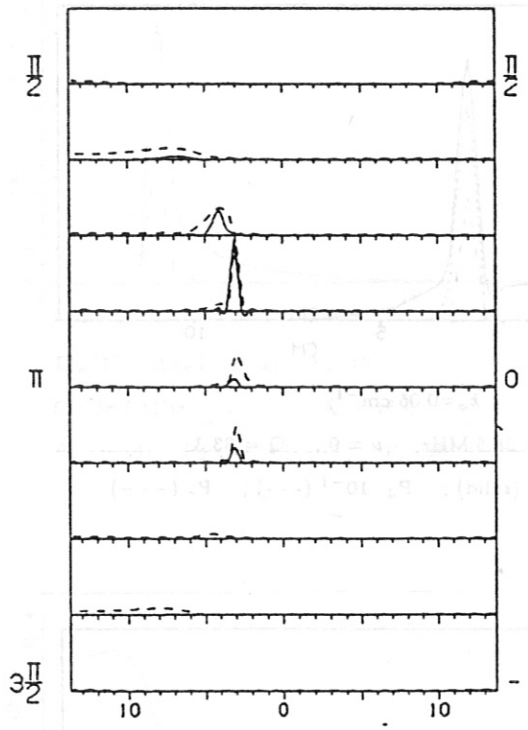

Fig(3) Ant.I a) $k_\phi = 0.$

$P_h^{max} = 2.75$; $E^{max} = 5.39 \cdot 10^1$

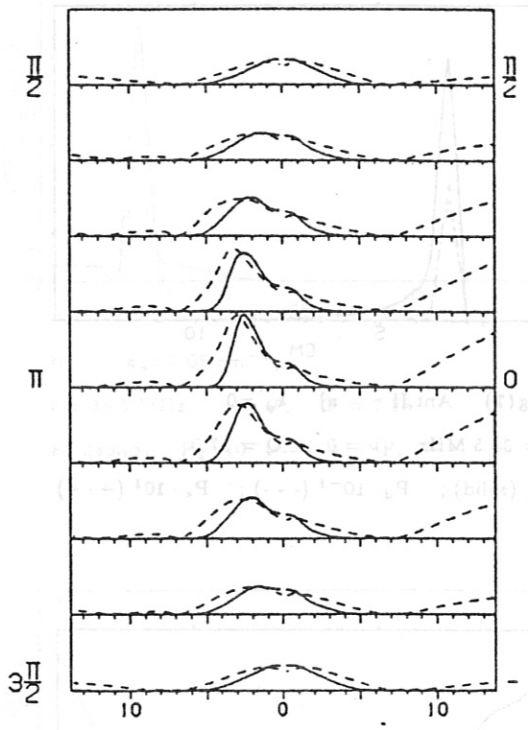

b) $k_\phi = 0.1\ cm^{-1}$

$P_h^{max} = 1.10 \cdot 10^{-1}$; $E^{max} = 2.36$

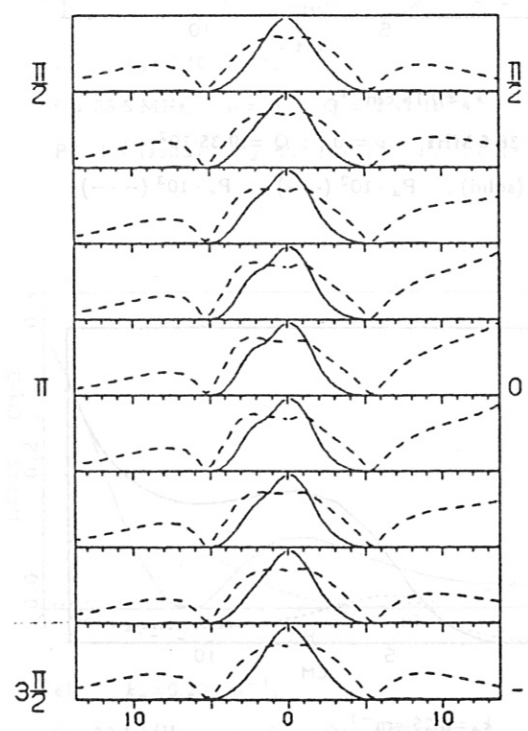

c) $k_\phi = 0.15\ cm^{-1}$

$P_h^{max} = 1.17 \cdot 10^{-1}$; $E^{max} = 1.84$

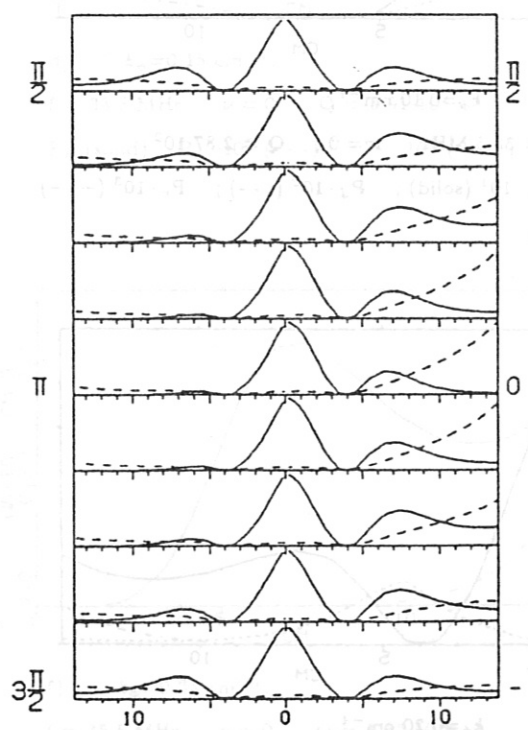

d) $k_\phi = 0.2\ cm^{-1}$

$P_h^{max} = 3.61 \cdot 10^{-4}$; $E^{max} = 1.73$

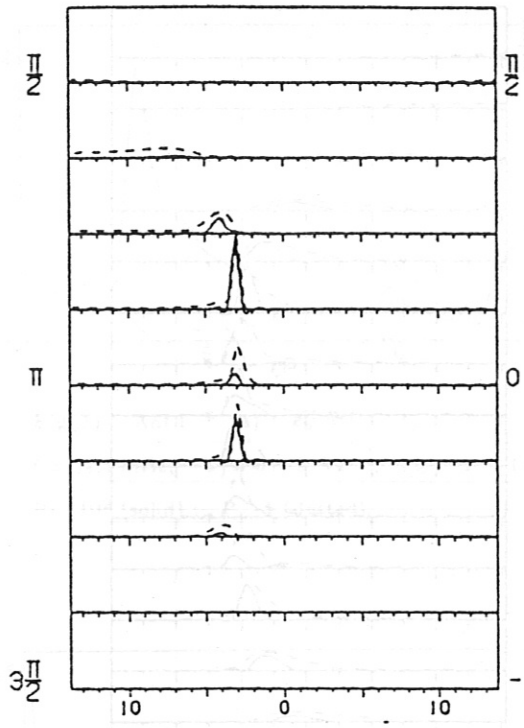

Fig(4) Ant.II a) $k_\phi = 0.$

$P_h^{max} = 4.53$; $E^{max} = 7.14 \cdot 10^1$

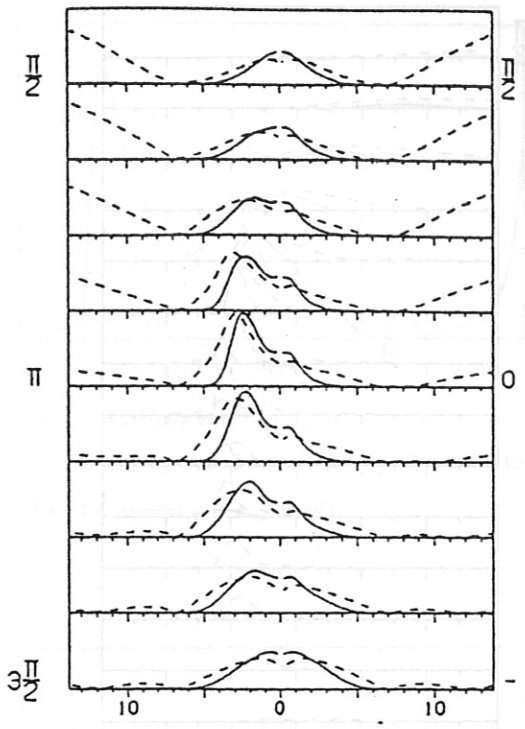

b) $k_\phi = 0.1\ cm^{-1}$

$P_h^{max} = 1.42 \cdot 10^{-1}$; $E^{max} = 2.60$

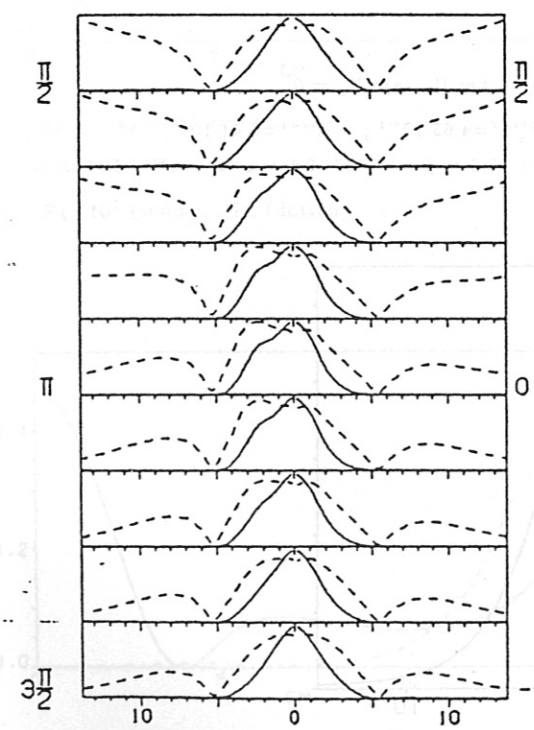

c) $k_\phi = 0.15\ cm^{-1}$

$P_h^{max} = 2.03 \cdot 10^{-1}$; $E^{max} = 2.03$

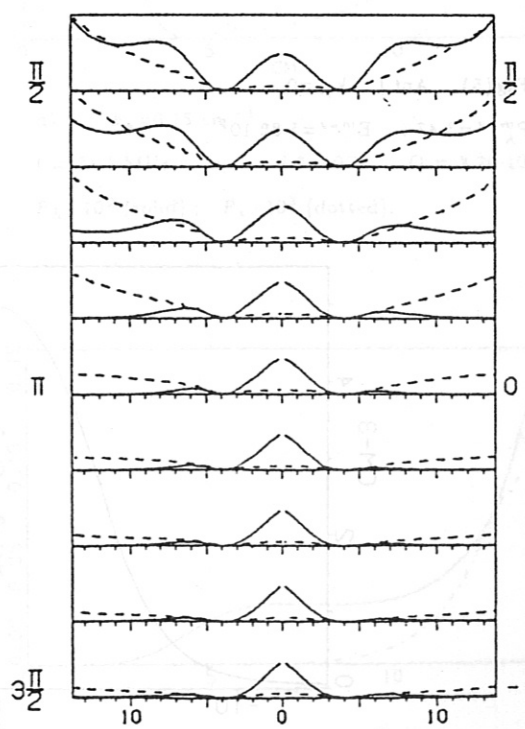

d) $k_\phi = 0.2\ cm^{-1}$

$P_h^{max} = 1.23 \cdot 10^{-3}$; $E^{max} = 1.86$

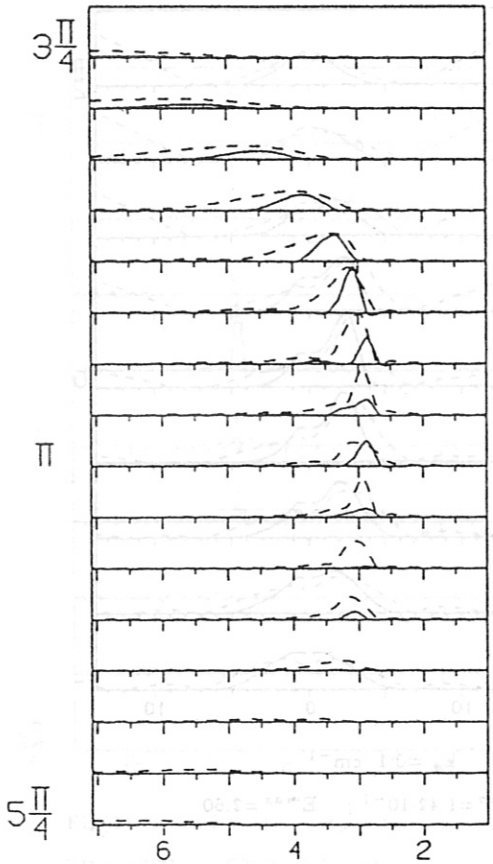

Fig(5) Ant.I $k_\phi = 0$.

$P_h^{max} = 3.47$; $E^{max} = 5.82 \cdot 10^1$

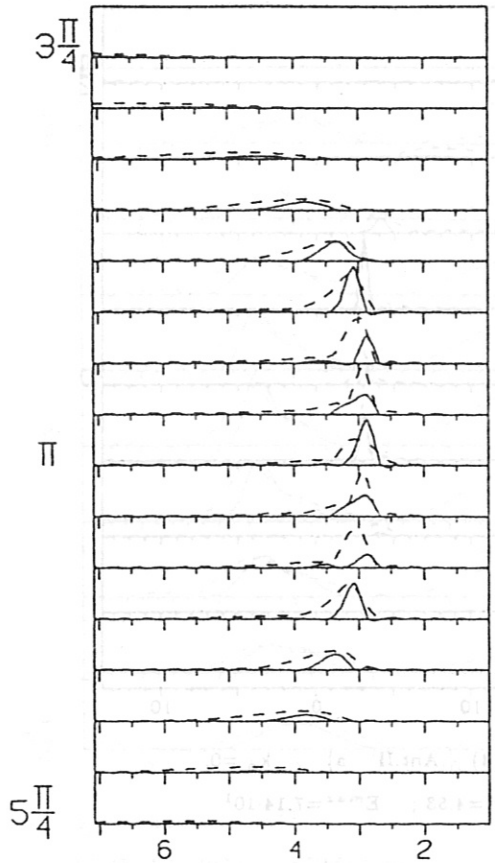

b) Ant.II a) $k_\phi = 0$

$P_h^{max} = 4.65 \cdot 10^{-1}$; $E^{max} = 8.44 \cdot 10^1$

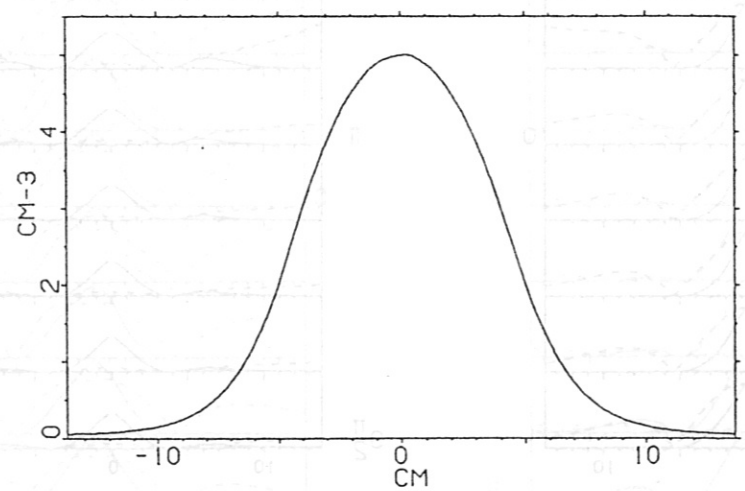

Fig(6) Plasma density profile

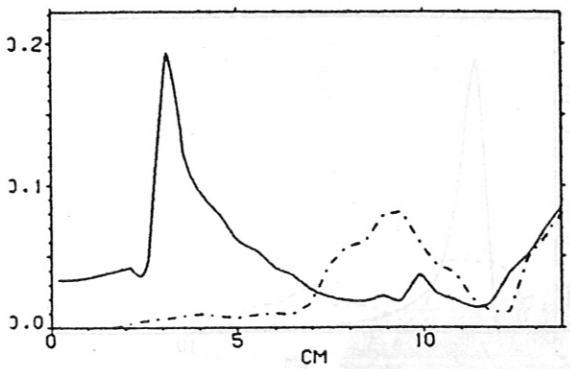

Fig(7) Ant.I a) $k_\phi = 0$,
f = 34.5 MHz, $\nu/\omega = 4.2 \cdot 10^{-4}$, Q = $1.77 \cdot 10^3$
$P_h \cdot 10^2$ (solid) ; $P_e \cdot 1$ (dotted).

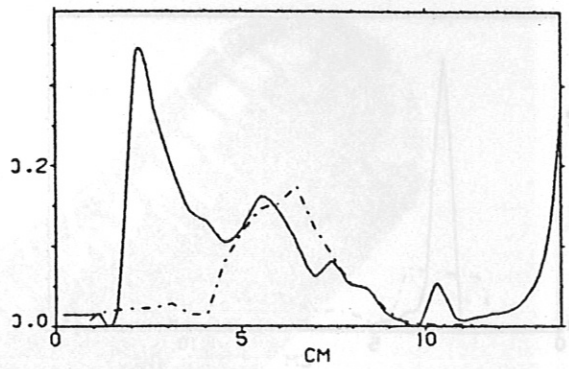

b) $k_\phi = 0.05$ cm^{-1} ,
f = 34.5 MHz, $\nu/\omega = 4.2 \cdot 10^{-4}$, Q = $5.27 \cdot 10^2$
$P_h \cdot 10^2$ (solid) ; P_e (dotted).

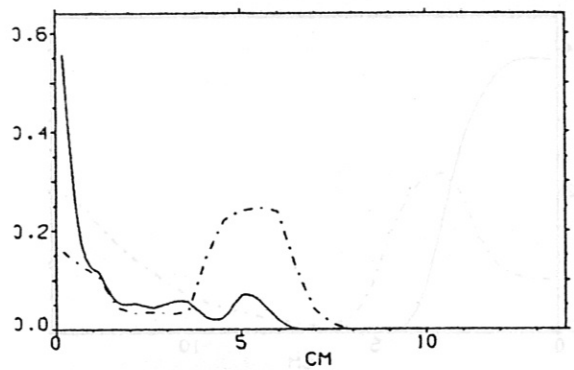

c) $k_\phi = 0.10$ cm^{-1} ,
f = 34.5 MHz, $\nu/\omega = 4.2 \cdot 10^{-4}$, Q = $2.76 \cdot 10^2$
$P_h \cdot 10^1$ (solid) ; P_e (dotted).

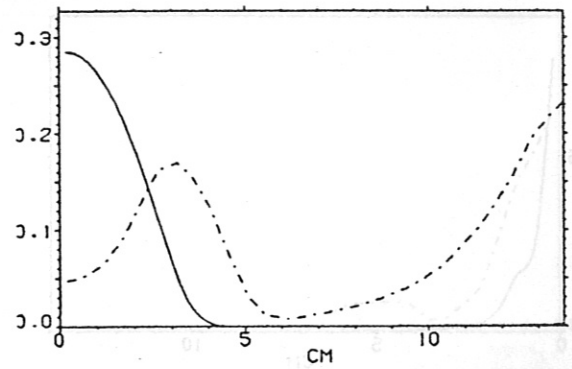

d) $k_\phi = 0.15$ cm^{-1} ,
f = 34.5 MHz, $\nu/\omega = 4.2 \cdot 10^{-4}$, Q = $2.20 \cdot 10^4$
$P_h \cdot 10^2$ (solid) ; $P_e \cdot 10^3$ (dotted).

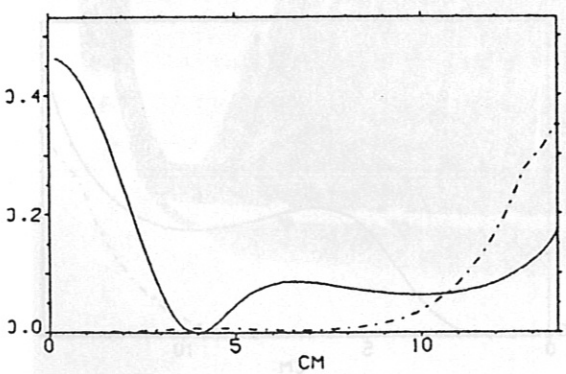

e) $k_\phi = 0.20$ cm^{-1} ,
f = 34.5 MHz, $\nu/\omega = 4.2 \cdot 10^{-4}$, Q = $9.36 \cdot 10^3$
$P_h \cdot 10^4$ (solid) ; $P_e \cdot 10^2$ (dotted).

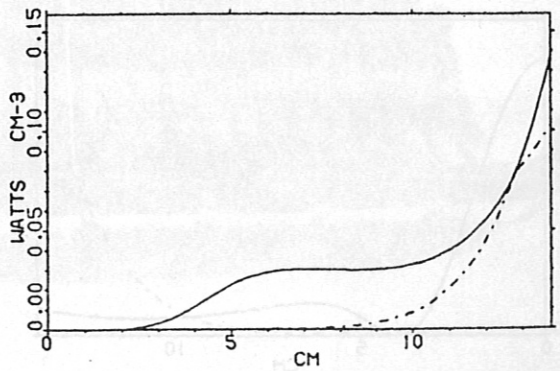

f) $k_\phi = 0.25$ cm^{-1} ,
f = 34.5 MHz, $\nu/\omega = 4.2 \cdot 10^{-4}$, Q = $1.30 \cdot 10^4$
$P_h \cdot 10^4$ (solid) ; $P_e \cdot 10^2$ (dotted).

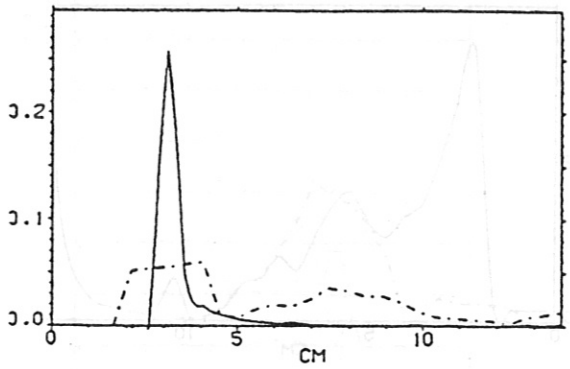

Fig(8) Ant.II a) $k_\phi = 0$,
f = 34.5 MHz, $\nu/\omega = 4.2 \cdot 10^{-4}$, Q = 17.7
P_h (solid) ; P_e (dotted).

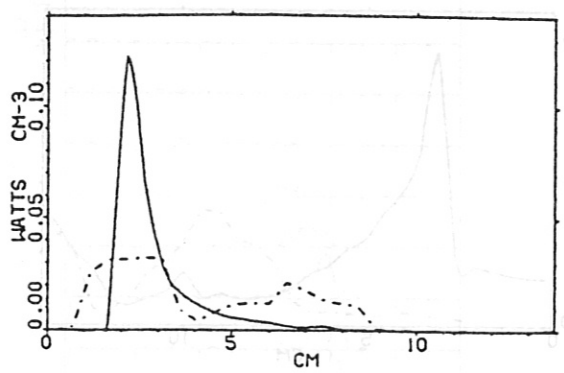

b) $k_\phi = 0.05$ cm^{-1} ,
f = 34.5 MHz, $\nu/\omega = 4.2 \cdot 10^{-4}$, Q = 37.6
P_h (solid) ; $P_e \cdot 10^{-1}$ (dotted).

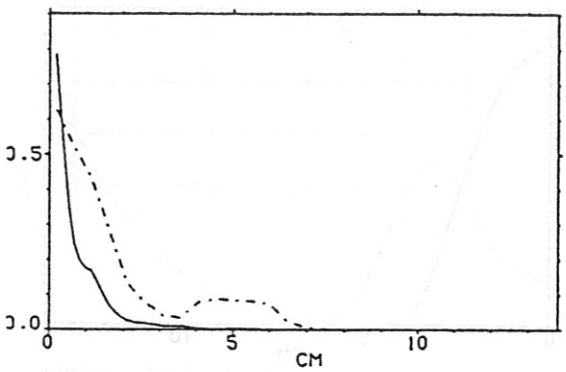

c) $k_\phi = 0.10$ cm^{-1} ,
f = 34.5 MHz, $\nu/\omega = 4.2 \cdot 10^{-4}$, Q = 50.4
P_h (solid) ; P_e (dotted).

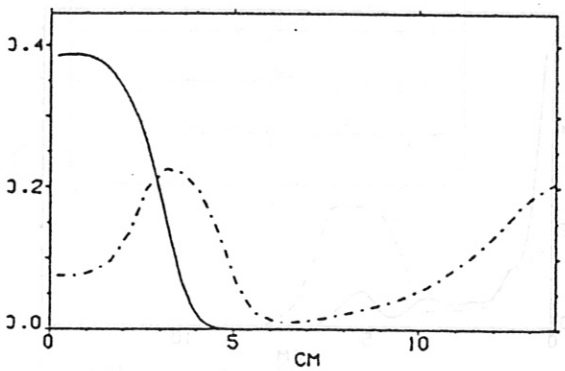

d) $k_\phi = 0.15$ cm^{-1} ,
f = 34.5 MHz, $\nu/\omega = 4.2 \cdot 10^{-4}$, Q = $3.29 \cdot 10^3$
$P_h \cdot 10^2$ (solid) ; $P_e \cdot 10^2$ (dotted)

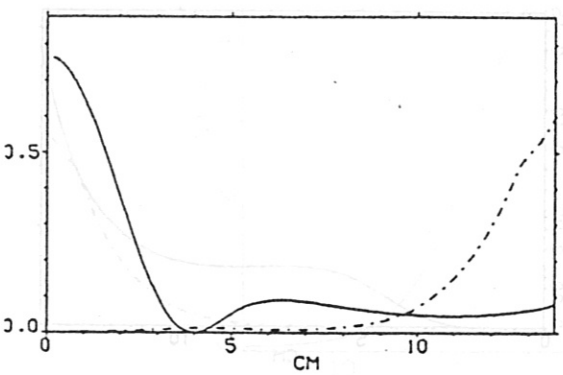

e) $k_\phi = 0.20$ cm^{-1} ,
f = 34.5 MHz, $\nu/\omega = 4.2 \cdot 10^{-4}$, Q = $8.78 \cdot 10^2$
$P_h \cdot 10^4$ (solid) ; $P_e \cdot 10^2$ (dotted).

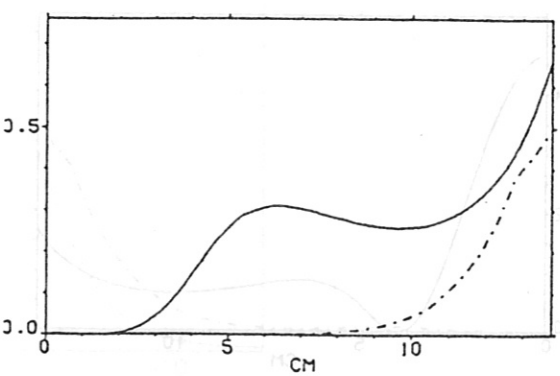

f) $k_\phi = 0.25$ cm^{-1} ,
f = 34.5 MHz, $\nu/\omega = 4.2 \cdot 10^{-4}$, Q = $1.29 \cdot 10^3$
$P_h \cdot 10^4$ (solid) ; $P_e \cdot 10^2$ (dotted)

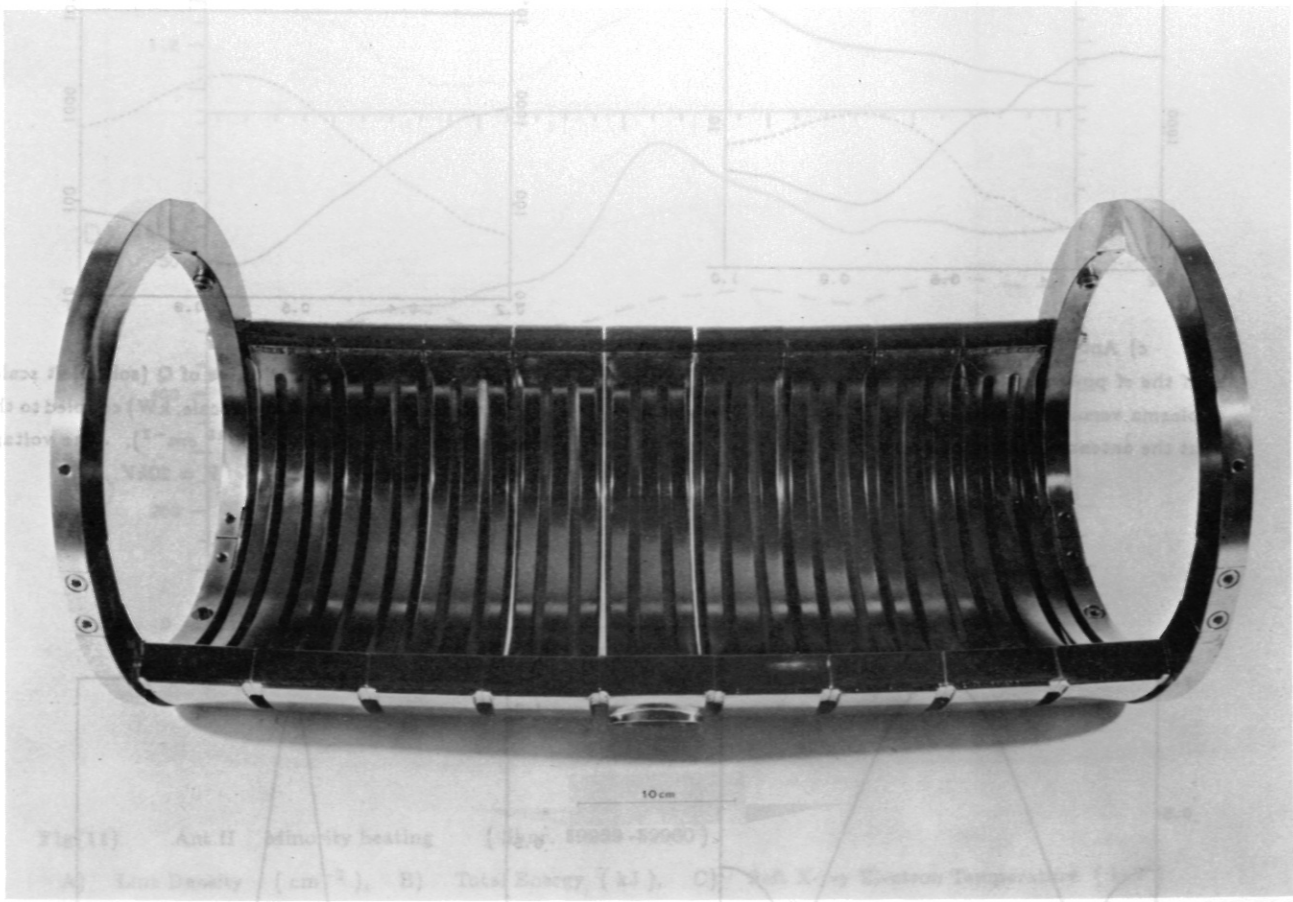

Fig. (9): Photo of the two antennas.

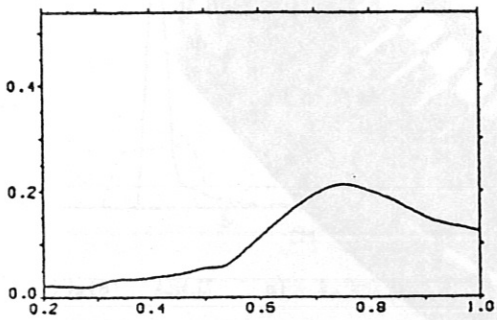

fig(10) a) Ant. I : evaluated resistive plasma loading (ohms) versus line density ($10^{-15}\ cm^{-2}$)

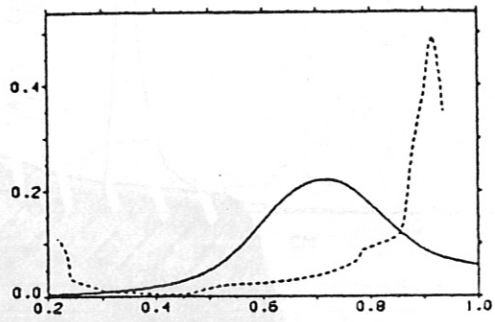

c) Ant. II : evaluated (solid) and measured (dotted) value of the resistive plasma loading (ohms) versus line density ($n \cdot 10^{-15}\ cm^{-2}$)

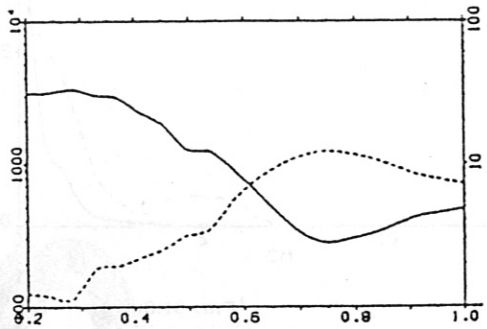

c) Ant. I : evaluated value of Q (solid, left scale) and of the rf power (dotted, right scale, kW) coupled to the plasma versus line density ($10^{-15}\ cm^{-2}$). The voltage at the antenna is assumed to be $V = 20kV$.

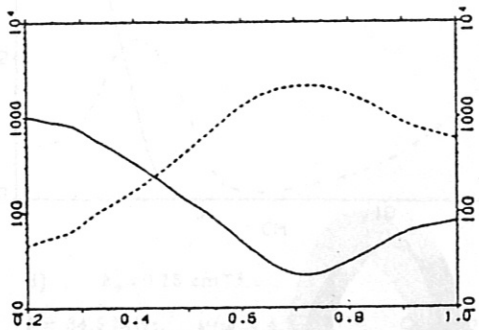

d) Ant. II : evaluated value of Q (solid, left scale) and of the rf power (dotted, right scale, kW) coupled to the plasma versus line density ($10^{-15}\ cm^{-2}$). The voltage at the antenna is assumed to be $V = 20kV$.

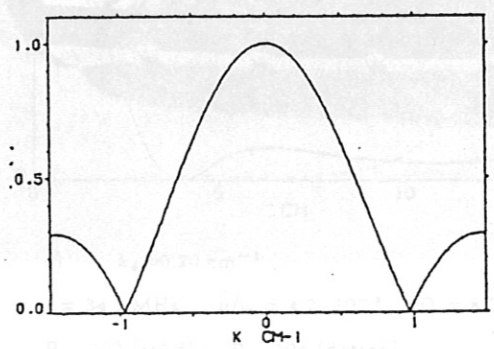

e) Ant. I : $J_\theta\ (k_\phi)$ versus $k_\phi\ (cm^{-1})$

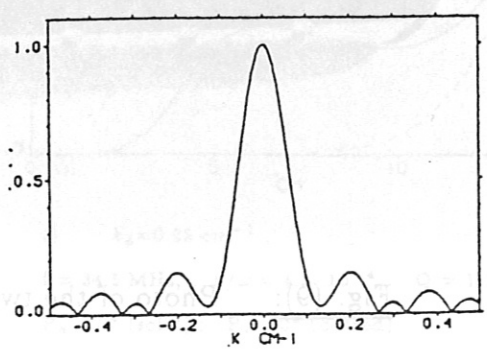

f) Ant. II : $J_\theta\ (k_\phi)$ versus $k_\phi\ (cm^{-1})$

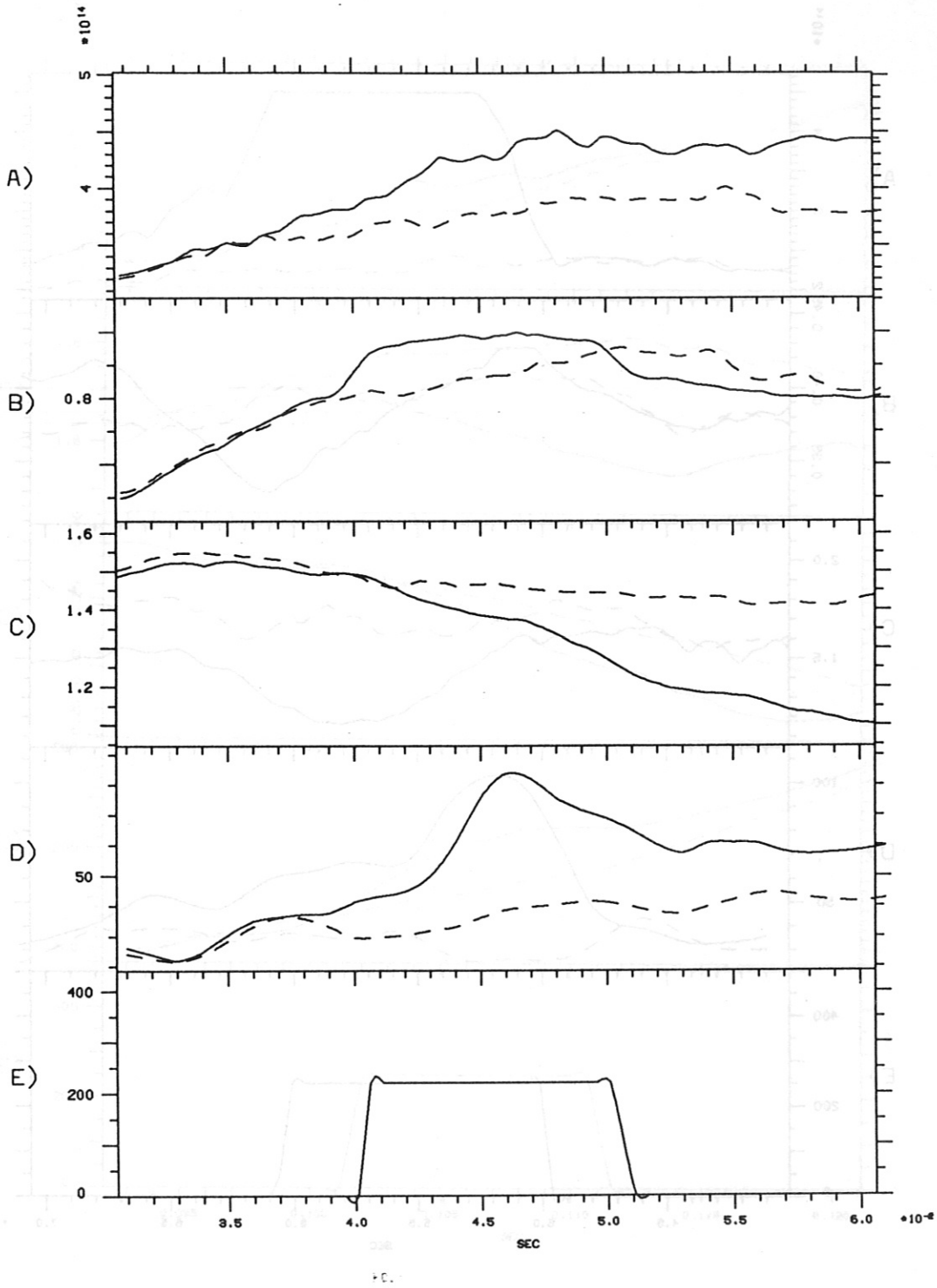

Fig(11) Ant.II Minority heating (Shnr. 59959 -59960)

A) Line Density (cm^{-2}), B) Total Energy (kJ), C) Soft X-ray Electron Temperature (keV)

D) Total Radiated Power (kW) , E) RF Power (kW) .

With rf, f=38.5 MHz, (solid) and without rf (dotted).

The time correlation with the rf pulse is falsed by the long integration time of the Bolometric signal ($\tau = 5$ ms).

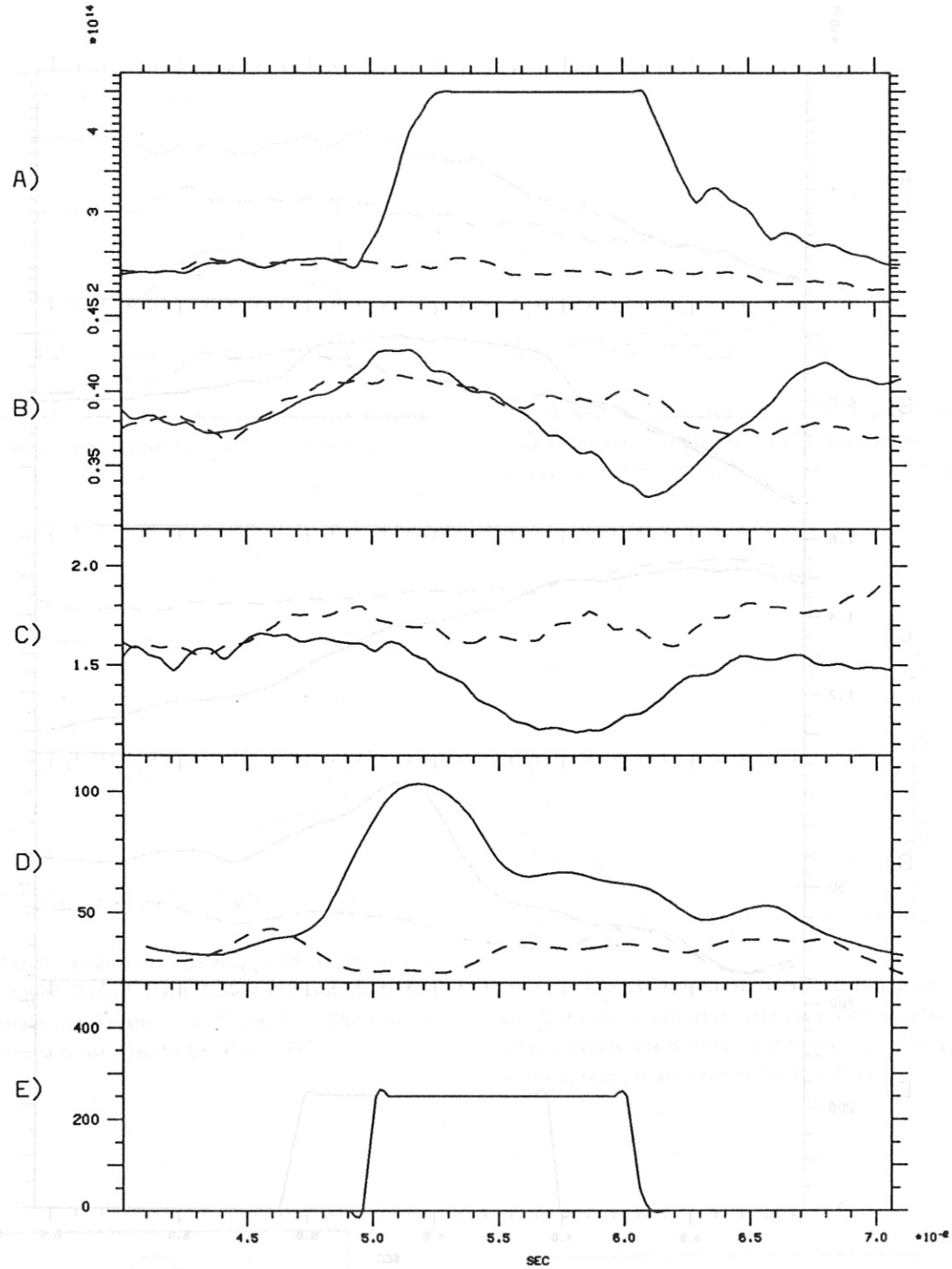

Fig(12) Ant.II Mode conversion (Shnr. 60128 -60129)

A) Line Density (cm^{-2}), B) Total Energy (kJ), C) Soft X-ray Electron Temperature (keV)

D) Total Radiated Power (kW) , E) RF Power (kW) .

With rf, f=34 MHz, (solid) and without rf (dotted).

The time correlation with the rf pulse is falsed by the long integration time of the Bolometric signal (τ = 5 ms).

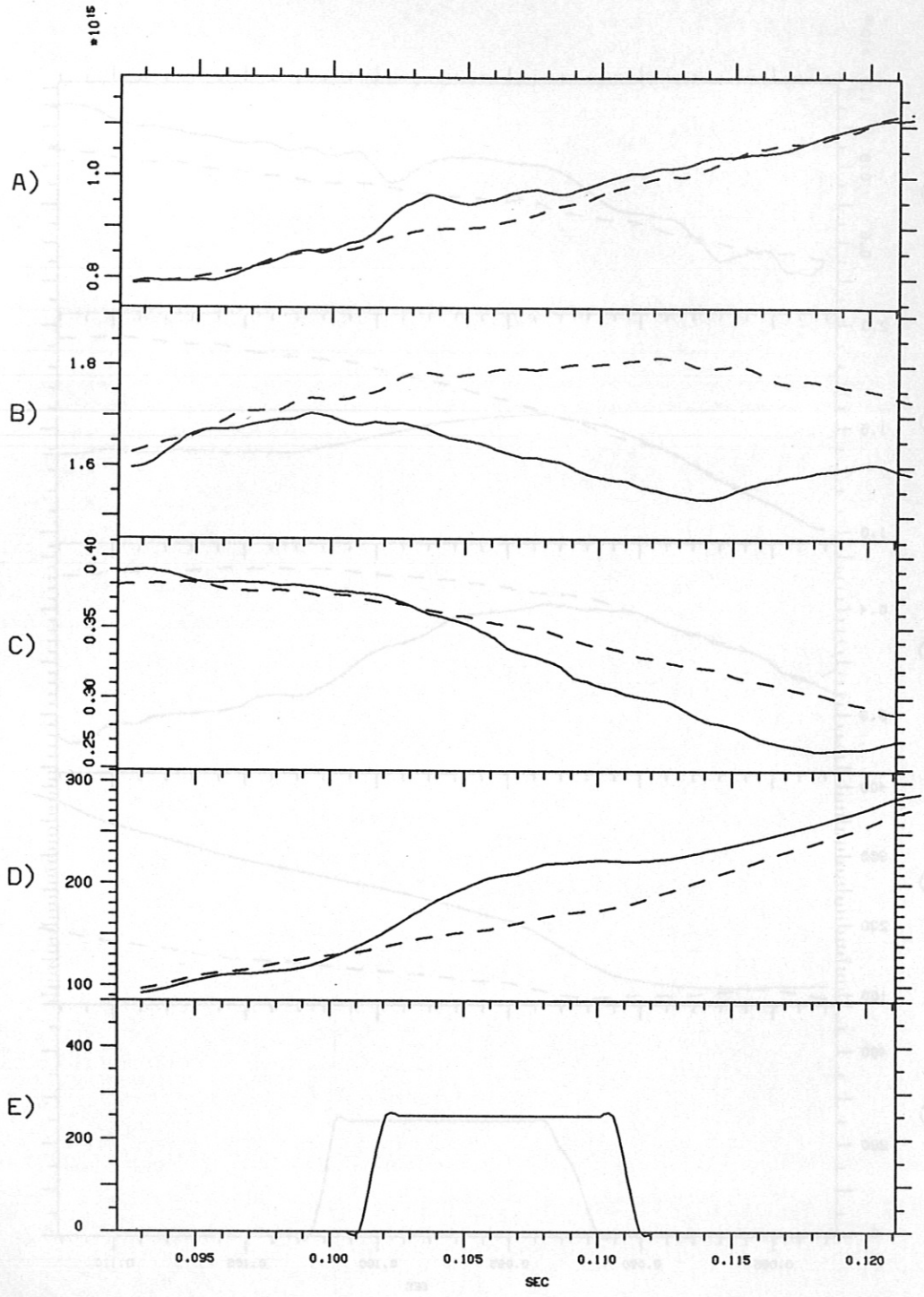

Fig(13) Ant.II Second harmonic (horizontal ellipse) (Shnr. 60284 -60285)

A) Line Density (cm^{-2}), B) Total Energy (kJ), C) Soft X-ray Electron Temperature (keV)

D) Total Radiated Power (kW) , E) RF Power (kW) .

With rf, f=77 MHz, (solid) and without rf (dotted).

The time correlation with the rf pulse is falsed by the long integration time of the Bolometric signal ($\tau = 5$ ms).

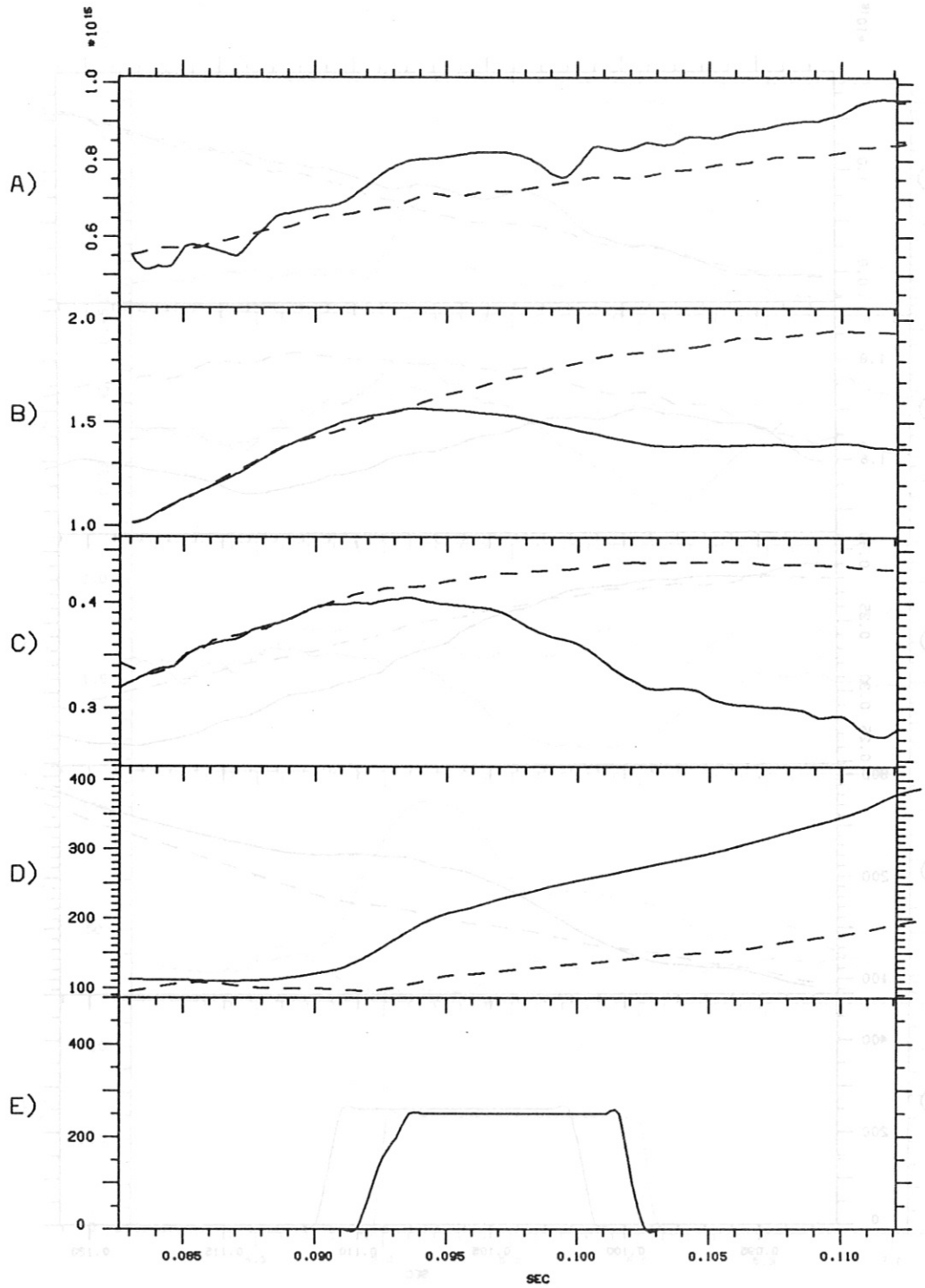

Fig(14) Ant.II Second harmonic (vertical ellipse) (Shnr. 60314 -60313)

A) Line Density (cm^{-2}), B) Total Energy (kJ), C) Soft X-ray Electron Temperature (keV)

D) Total Radiated Power (kW) , E) RF Power (kW) .

With rf, f=77 MHz, (solid) and without rf (dotted).

The time correlation with the rf pulse is falsed by the long integration time of the Bolometric signal (τ = 5 ms).